1521-0111/99/3/184–196$35.00
MOLECULAR PHARMACOLOGY

https://doi.org/10.1124/molpharm.120.000116
Mol Pharmacol 99:184–196, March 2021

Nelfinavir and Its Active Metabolite M8 Are Partial Agonists and Competitive Antagonists of the Human Pregnane X Receptor[S]

Oliver Burk, Thales Kronenberger,[1] Oliver Keminer, Serene M. L. Lee, Tobias S. Schiergens, Matthias Schwab, and Björn Windshügel

Dr. Margarete Fischer-Bosch-Institute of Clinical Pharmacology, Stuttgart, and University of Tübingen, Tübingen, Germany (O.B., M.S.); Fraunhofer Institute for Molecular Biology and Applied Ecology IME, ScreeningPort, Hamburg, Germany (T.K., O.K., B.W.); Biobank of the Department of General, Visceral, and Transplantion Surgery, University Hospital, Ludwig-Maximilians University, Munich, Munich, Germany (S.M.L.L., T.S.S.); Departments of Clinical Pharmacology, and Pharmacy and Biochemistry, University of Tübingen, Tübingen, Germany (M.S.); and Department of Chemistry, Institute for Biochemistry and Molecular Biology, Universität Hamburg, Hamburg, Germany (B.W.)

Received July 14, 2020; accepted December 21, 2020

ABSTRACT

The HIV protease inhibitor nelfinavir is currently being analyzed for repurposing as an anticancer drug for many different cancers because it exerts manifold off-target protein interactions, finally resulting in cancer cell death. Xenosensing pregnane X receptor (PXR), which also participates in the control of cancer cell proliferation and apoptosis, was previously shown to be activated by nelfinavir; however, the exact molecular mechanism is still unknown. The present study addresses the effects of nelfinavir and its major and pharmacologically active metabolite nelfinavir hydroxy-*tert*-butylamide (M8) on PXR to elucidate the underlying molecular mechanism. Molecular docking suggested direct binding to the PXR ligand-binding domain, which was confirmed experimentally by limited proteolytic digestion and competitive ligand-binding assays. Concentration-response analyses using cellular transactivation assays identified nelfinavir and M8 as partial agonists with EC_{50} values of 0.9 and 7.3 μM and competitive antagonists of rifampin-dependent induction with IC_{50} values of 7.5 and 25.3 μM, respectively. Antagonism exclusively resulted from binding into the PXR ligand-binding pocket. Impaired coactivator recruitment by nelfinavir as compared with the full agonist rifampin proved to be the underlying mechanism of both effects on PXR. Physiologic relevance of nelfinavir-dependent modulation of PXR activity was investigated in respectively treated primary human hepatocytes, which showed differential induction of PXR target genes and antagonism of rifampin-induced ABCB1 and CYP3A4 gene expression. In conclusion, we elucidate here the molecular mechanism of nelfinavir interaction with PXR. It is hypothesized that modulation of PXR activity may impact the anticancer effects of nelfinavir.

SIGNIFICANCE STATEMENT

Nelfinavir, which is being investigated for repurposing as an anticancer medication, is shown here to directly bind to human pregnane X receptor (PXR) and thereby act as a partial agonist and competitive antagonist. Its major metabolite nelfinavir hydroxy-*tert*-butylamide exerts the same effects, which are based on impaired coactivator recruitment. Nelfinavir anticancer activity may involve modulation of PXR, which itself is discussed as a therapeutic target in cancer therapy and for the reversal of chemoresistance.

Introduction

The HIV protease inhibitor nelfinavir is no longer commonly used in modern antiretroviral therapy of AIDS because of the introduction of more efficacious medications. However, it is a promising candidate for repurposing as an anticancer drug for many different cancers [for review, see Shim and Liu (2014) and Bhattarai et al. (2016)]. This is because of the manifold off-target interactions of nelfinavir, which not only targets HIV protease but also inhibits, among others, the activities of 20S proteasome (Gupta et al., 2007), cyclin-dependent protein kinase (CDK) 2 (Jiang et al., 2007), site-2-protease (Guan et al., 2011), and heat shock protein 90 (Shim et al., 2012). Proteome-wide in silico analysis of nelfinavir potential off-target interactions suggested the interaction with and possible inhibition of multiple protein kinases (Xie et al., 2011). Because of these interactions, nelfinavir results in diverse effects on cancer cells, such as inhibition of the PI3K-AKT-mTOR pathway and induction of endoplasmic reticulum stress, which finally lead to cell death by cell cycle arrest, triggering of the unfolded protein response, apoptosis, and autophagy (Koltai, 2015). The major and antivirally equipotent metabolite hydroxy-*tert*-butylamide (Zhang et al., 2001),

Some information presented herein is in the Ph.D. thesis of T.K.: Kronenberger T (2017) *Targeting alternative ligand-binding sites in nuclear receptors using computational and experimental screening*. Ph.D. thesis, University of São Paulo, São Paulo, Brazil (published online at https://www.teses.usp.br/teses/disponiveis/42/42135/tde-17112017-102040/en.php).

This work was supported by the Robert Bosch Foundation, Stuttgart, Germany (M.S., O.B.) and the Hamburg Ministry of Science, Research and Equality of the Free and Hanseatic City of Hamburg (B.W.). T.K. was supported by Fundação de Amparo à Pesquisa do Estado de São Paulo (FAPESP) [Grants 2014/03644-9 and 2014/27313-1].

[1]Current affiliation: Department of Internal Medicine VIII, University Hospital Tübingen, Tübingen, Germany and School of Pharmacy, University of Eastern Finland, Kuopio, Finland.

https://doi.org/10.1124/molpharm.120.000116.

[S] This article has supplemental material available at molpharm.aspetjournals.org.

also designated as M8, demonstrated in vitro antitumor activity comparable with that of the parent compound (Guan et al., 2011). M8 likely contributes to total nelfinavir antiviral and anticancer activity, as its concentrations in human plasma reach up to one-third of those of nelfinavir (Zhang et al., 2001).

The nuclear receptor (NR) pregnane X receptor (PXR) (NR1I2) is one of the many targets of nelfinavir. In response to xenobiotics, PXR transcriptionally regulates the expression of cytochrome P450 drug-metabolizing enzymes and drug transporters, such as CYP3A4 and P-glycoprotein (multidrug resistance protein 1/ABCB1). Since nelfinavir-dependent induction of the respective genes and proteins was demonstrated in rats (Huang et al., 2001), primary human hepatocytes (Dixit et al., 2007; Liu et al., 2012), and the human colorectal adenocarcinoma cell lines LS174T and LS180 (Huang et al., 2001; Gupta et al., 2008), it is assumed that nelfinavir activates PXR. However, inconsistent results were obtained when analyzing nelfinavir-dependent PXR activation using cellular transactivation assays. Although nelfinavir did not activate PXR in a one-hybrid reporter gene assay in monkey kidney fibroblast CV-1 cells (Dussault et al., 2001), it induced PXR-dependent activation of CYP3A4 and CYP2B6 promoter reporter genes in human hepatocellular carcinoma HepG2 cells (Svärd et al., 2010; Lynch et al., 2015). In contrast, knockdown experiments in LS180 cells clearly attributed the nelfinavir-dependent induction of CYP3A4 and ABCB1 gene expression to PXR (Gupta et al., 2008). However, because former work had also demonstrated that nelfinavir neither bound to the PXR ligand-binding domain (LBD) in vitro nor recruited coactivator mediator complex subunit 1 (MED1) to PXR in a mammalian two-hybrid assay (Dussault et al., 2001), the molecular mechanism of nelfinavir-dependent PXR activation remains obscure. As mentioned above, nelfinavir was shown to inhibit CDK2 activity and is further supposed to also inhibit CDK5 and cAMP-dependent protein kinase (Xie et al., 2011), which have all been shown to phosphorylate PXR in vitro and thereby inhibit its transactivation activity [for a review, see Mackowiak and Wang (2016)]. Altogether, published data do not provide evidence for direct binding of nelfinavir to PXR and are consistent with a putative indirect activation mechanism of the drug, which may rely on the inhibition of inhibitory protein kinases.

Given the current efforts to repurpose nelfinavir as an anticancer drug, it is of interest that PXR is discussed as a therapeutic target in anticancer therapy. Depending on the cancer entity, PXR activation may either result in tumor progression and promote chemoresistance or suppress cancer cell growth (Pondugula et al., 2016; Xing et al., 2020). In the latter case, PXR activation may contribute to nelfinavir's anticancer activity. A thorough understanding of how exactly the drug affects PXR activity will promote our knowledge on the potential of nelfinavir as an anticancer drug.

We aim here to elucidate the molecular mechanism of nelfinavir-dependent activation of PXR and to investigate the PXR interaction properties of the pharmacologically equipotent major metabolite M8. By using a combination of biochemical and cellular assays as well as in silico molecular modeling, it is shown that nelfinavir and M8 bind to human PXR and act both as partial agonists and competitive antagonists. Impaired recruitment of coactivators mainly accounts for these properties. Studies in primary human hepatocytes demonstrate the physiologic relevance of nelfinavir's agonism and antagonism of PXR; however, nelfinavir exhibits differential induction of PXR target genes. The chemical structure of nelfinavir may thus represent a suitable starting point for the development of PXR-selective modulators.

Materials and Methods

Chemicals and Biological Reagents. Rifampin was purchased from Merck Chemicals (Darmstadt, Germany); Tocris Bioscience (Bristol, UK) provided T0901317, GW4064, and SR12813; nelfinavir and M8 were purchased from Toronto Research Chemicals (North York, Canada); DMSO, GW3965, triiodo-L-thyronine, and 1α,25-dihydroxyvitamin D3 were provided by Sigma-Aldrich (Munich, Germany); and rosiglitazone and CITCO were purchased from Sellekchem (Houston, TX) and ENZO Life Sciences (Lörrach, Germany), respectively. SPA70 was provided by Axon Medchem (Groningen, The Netherlands). Cell culture medium and supplements were obtained from Life Technologies (Darmstadt, Germany).

Plasmids. Eukaryotic expression plasmids encoding full-length human nuclear receptors PXR (Geick et al., 2001), constitutive androstane receptor (CAR) 1 (Burk et al., 2002), CAR3 (Arnold et al., 2004), thyroid hormone receptor α1, thyroid hormone receptor β1, vitamin D receptor (VDR) (Burk et al., 2005), liver X receptor (LXR) α, and LXRβ (Piedade et al., 2015) have all been described. Expression plasmids encoding the human small PXR variant, which consists of the ligand-binding domain (amino acids 113–434) only (Jeske et al., 2017), and PXR mutant S208W/S247W/C284W (Burk et al., 2018) have already been described. T. Tanaka kindly provided the human peroxisome proliferator–activated receptor (PPAR) γ1 expression plasmid (Tachibana et al., 2005). Farnesoid X receptor (FXR) α2 expression plasmid was constructed by cloning the respective open reading frame amplified by polymerase chain reaction (PCR) from the cDNA of primary human hepatocytes using appropriate primers into expression vector pcDNA3 (Thermo Fisher Scientific Invitrogen, Carlsbad, CA). The 5′ upstream primer additionally introduced an optimized Kozak consensus sequence. Sequencing identified an FXR clone lacking the 12-bp insertion, which encodes amino acids MYTG (i.e., FXRα2).

Expression plasmids encoding fusion proteins of the GAL4–DNA-binding domain (DBD) and the receptor interaction domains (RIDs) of nuclear receptor coactivator (NCOA) 1 (residues 583–783), NCOA2 (residues 583–779), MED1 (residues 527–774) (Arnold et al., 2004), and nuclear receptor corepressor 2 (NCOR2), (residues 1109–1330) or helix 1 part of the LBD of PXR (residues 132–188) as well as expression plasmids encoding fusion proteins of the VP16 activation domain (AD) and the whole or part of the PXR-LBD (residues 108–434

ABBREVIATIONS: ABCB1, ATP-binding cassette B1; AD, activation domain; AF-2, activation function 2; AKR1B10, aldo-keto reductase 1B10; CAR, constitutive androstane receptor; CDK, cyclin-dependent protein kinase; CI, confidence interval; DBD, DNA-binding domain; EPHX1, epoxide hydrolase 1; FASN, fatty acid synthase; FRET, fluorescence resonance energy transfer; FXR, farnesoid X receptor; HTCR, Human Tissue and Cell Research; ID, identifier; LBD, ligand-binding domain; LBP, ligand-binding pocket; LXR, liver X receptor; M8, nelfinavir hydroxy-*tert*-butylamide; MDR1, multidrug resistance protein 1; MED1, mediator complex subunit 1; MOE, Molecular Operating Environment; NCOA, nuclear receptor coactivator; NCOR2, nuclear receptor corepressor 2; NFV, nelfinavir; NR, nuclear receptor; PCR, polymerase chain reaction; PDB, Protein Data Bank; PPAR, peroxisome proliferator–activated receptor; PXR, pregnane X receptor; RID, receptor interaction domain; RIF, rifampin; RMS, root-mean-square; rRNA, ribosomal RNA; SMPDL3A, sphingomyelin phosphodiesterase acid–like 3A; Tk, thymidine kinase; TR-FRET, time-resolved FRET; UGT1A3, UDP-glucuronosyltransferase 1A3; VDR, vitamin D receptor.

and 189–434, respectively) (Burk et al., 2005) have been described. The expression plasmid encoding the fusion protein of GAL4-DBD with PXR-LBD (residues 108–434) was constructed by subcloning the insert of pVP16-AD/PXR-LBD(108–434) into pM (Takara Bio Clontech, Mountain View, CA).

Firefly luciferase reporter gene plasmids have previously been described: CYP3A4 enhancer/promoter reporter gene plasmid pGL4-CYP3A4(7830/Δ7208-364) (Burk et al., 2018); CYP2B6 enhancer/promoter reporter gene plasmid pB-1.6k/PB/XREM, as provided by H. Wang (Wang et al., 2003); reporter gene plasmid comprising a dimer of the MDR1-DR4(I) motif (Geick et al., 2001); pGL3(DR3)$_3$Tk (Hustert et al., 2001); plasmid PPRE X3-Tk-luc(1015; Addgene plasmid), as provided by B. Spiegelman (Forman et al., 1995); reporter gene plasmid containing a dimer of the consensus nuclear receptor inverted repeat 1 motif (Piedade et al., 2015); and GAL4-dependent reporter gene plasmid pGL3-G5 (Arnold et al., 2004). With the exception of the CYP3A4 and CYP2B6 reporters and pGL3-G5, the other reporter gene plasmids harbor the thymidine kinase minimal promoter. The *Renilla* luciferase expression plasmid pGL4.75[hRluc/CMV] (Promega, Madison, WI) has been used.

Molecular Docking. Three-dimensional coordinates for nelfinavir and its metabolite M8 were generated within MOE version 2019.01.02 (Chemical Computing Group Inc., Montreal, Canada). All PXR X-ray crystal structures were downloaded from the Protein Data Bank (Berman et al., 2000). Based on a structural analysis of all available PXR X-ray crystal structures using PROCHECK and ProSa (Laskowski et al., 1993; Sippl, 1993), PDB IDs 1M13, 1NRL, and 2O9I were selected for docking. For 1M13, two separate structures with different alternate atoms for Cys284 were generated, and both chains of 1NRL and 2O9I were selected, resulting in an ensemble of six LBD structures. The mutation C284S in 2O9I was mutated back into the wild-type residue using MOE, and solvent atoms were removed. All structures were superposed on Cα atoms of amino acids lining the ligand-binding pocket (LBP). Protein structures were prepared using Protonate3D in MOE and energy-minimized (Amber10:EHT force field with R-Field implicit solvation model) using a three-step procedure (Cα atoms, backbone, all atoms) with a tether of 0.5 and a root-mean-square (RMS) gradient of 5. Potential alternative ligand-binding sites on the LBD surface were identified by applying Site Finder in MOE. Compounds were docked using GOLD version 5.8.1 (Cambridge Crystallographic Data Centre, Cambridge, UK). The docking search space for the LBP was defined by a sphere of 13 Å radius centered on coordinates of atom C27 of the ligand hyperforin (PDB ID: 1M13), whereas for the AF-2 site, a sphere of 10 Å radius centered on atom CD2 of Leu670 (PDB ID: 1NRL, chain C) was used. The docking search space for the alternative sites was defined by the amino acids lining the pockets. For each compound, 100 docking runs were conducted. The early termination option was switched off.

Limited Proteolytic Digestion. Radiolabeled PXR-LBD protein (residues 113–434) was synthesized in vitro using the TNT T7 Quick Coupled Transcription/Translation System (Promega) as recommended by the manufacturer. Briefly, 50-μl reactions were set up with 40 μl TNT T7 Quick Master Mix, 20 μCi ^{35}S-methionine (specific activity > 1000 Ci/mmol; Hartmann Analytic, Braunschweig, Germany) and 1 μg of the small PXR expression plasmid. Five-microliter aliquots thereof were preincubated with compounds or solvent DMSO for 30 minutes and then subjected to proteolytic digestion with trypsin for 10 minutes as described (Jeske et al., 2017). Reactions were separated on 12% SDS polyacrylamide gels, which were subsequently stained with Coomassie, dried, and exposed to BAS-IP MS 2325 imaging plates (Fuji, Kanagawa, Japan). Input PXR-LBD protein and protected proteolytic fragments were detected by scanning the imaging plates with the CR35 Bio radioluminography laser scanner (Raytest, Straubenhardt, Germany) and quantified using AIDA software version 4.50.010 (Raytest). Each independent experiment was performed in technical single replicates.

Competitive Ligand Binding. Ligand binding to PXR was investigated using the LanthaScreen TR-FRET PXR (SXR) competitive binding assay kit (PV4839, lot 2109118; Thermo Fisher Scientific, Waltham, MA). All assay steps and the detection were carried out according to the protocol and microplate reader-specific guidelines of the manufacturer. In brief, the assay was performed in a volume of 20 μl per well of 384-well, black, nonbinding, low-volume plates (Corning Life Sciences, Amsterdam, The Netherlands) with 2.5 nM glutathione-*S*-transferase–PXR-LBD, 40 nM Fluormone PXR Green, and 10 nM terbium-labeled anti–glutathione-*S*-transferase antibody. Positive control (SR12813) and test compounds nelfinavir and M8 were added at concentrations ranging from 0.5 nM to 30 μM. Reactions were incubated for 60 minutes at room temperature in the dark. The fluorescent emissions were measured on an Infinite M1000 multimode microplate reader (Tecan, Männedorf, Switzerland) at 486 and 515 nm. All measurements were optimized using maximum signal control reactions [100 μs lag time, 200 μs integration, flash mode 2 (100 Hz, ~8 joule)]. The FRET ratio was calculated by dividing the emission signal at 515 nm by that at 486 nm. Two-percent DMSO was used as the negative control (0% relative binding) and 30 μM SR-12813 as the positive control (100% relative binding). The data were expressed as relative binding (%) [relative binding (%) = 100% × (DMSO FRET ratio – compound FRET ratio)/(DMSO FRET ratio − 30 μM SR12813 FRET ratio)], according to Dong et al. (2010).

Cell Culture. HepG2 cells (HB-8065, lot number 58341723; American Type Culture Collection, Manassas, VA) and H-P cells, which represent a HepG2 cell clone stably overexpressing human PXR (Bitter et al., 2015), were cultivated in minimal essential medium supplemented with 10% FBS, 2 mM L-glutamine, 100 U/ml penicillin, and 0.1 mg/ml streptomycin. In drug treatments, dextran-coated charcoal-stripped FBS replaced regular FBS. Both cell lines were routinely checked for contamination with mycoplasma by PCR (VenorGeM Classic; Minerva Biolabs, Berlin, Germany).

Concentration-Response Analyses. Transient transfections of H-P cells were set up according to the batch protocol for jetPEI (Polyplus, Illkirch, France). Transfected cells were seeded in 96-well Cell+ flat-bottom microplates (Sarstedt, Nümbrecht, Germany) using per well 250 μl of a suspension consisting of 200 μl H-P cells (4×10^4 cells) and 50 μl transfection mixture containing 0.3 μg CYP3A4 reporter gene plasmid, 0.01 μg pGL4.75[hRluc/CMV], and 0.6 μl jetPEI transfection reagent in 150 mM NaCl. Twenty-four hours after transfection, cells were treated with varying concentrations of chemicals ranging from 0.03 to 10 μM (nelfinavir and M8) or 30 μM (rifampin) in the presence or absence of fixed concentrations of competing ligands for another 24 hours in a volume of 100 μl. Then culture medium was removed, and cells were lysed with 50 μl of 1× passive lysis buffer (Promega). Firefly and *Renilla* luciferase assays were performed separately with 10 μl lysate each in white opaque 96-well microplates (OptiPlate-96; Perkin-Elmer) by adding 150 or 100 μl of respective assay solutions, which have been described previously (Geick et al., 2001; Piedade et al., 2015). Luminescence was measured after 10-minute incubation at constant shaking with the 2300 EnSpire multimode plate reader (Perkin Elmer, Rodgau, Germany) for 0.1 seconds. Concentration-response experiments were done five to seven times independently, each in technical triplicates.

Nuclear Receptor Specificity, Mammalian Two-Hybrid, and Mutant PXR Assays. Transient transfections were performed in 24-well plates with 1.5×10^5 HepG2 cells per well seeded the day before, using per well 1 μl jetPRIME transfection reagent (Polyplus) and a plasmid DNA mixture consisting of 0.04 μg of the respective NR expression plasmids, 0.3 μg corresponding firefly luciferase reporter gene constructs, and 0.005 μg pGL4.75[hRluc/CMV] filled up with pUC18 to 0.5 μg. The following reporter gene plasmids were used for the NR specificity tests: CYP3A4 reporter (PXR) and CYP2B6 reporter (CAR1, CAR3), MDR1-DR4 reporter (LXRα, LXRβ, TRα1, TRβ1), DR3 reporter (VDR), PPRE ×3 Tk-luc (PPARγ1), and consensus inverted repeat 1 reporter (FXRα2). In the antagonist mode, the following prototypical agonists were further used: 10 μM rifampin (PXR), 10 μM CITCO (CAR3), 2 μM GW3965 (LXRα, LXRβ), 1 μM triiodo-L-thyronine (TRα1, TRβ1), 0.1 μM 1α,25-dihydroxyvitamin D3 (VDR),

1 μM rosiglitazone (PPARγ1), and 1 μM GW4064 (FXRα2). Transfections for mammalian two-hybrid PXR corepressor, coactivator, and LBD assembly assays were set up similarly, using the plasmids specified in the legend of Fig. 6. In mutant PXR assays, respective PXR expression plasmids were combined with the CYP3A4 reporter as described above. Twenty hours after transfection, cells were treated with chemicals for another 24 hours. Cell lysis and reporter gene assays were performed as described above. All transfections were done four to five times independently, each in technical triplicates and with at least two different preparations of plasmids.

Human Liver Tissue Samples and Primary Human Hepatocytes. Double-coded human liver samples and corresponding data used in this study were provided by the Biobank of the Department of General, Visceral, and Transplantation Surgery in Ludwig-Maximilians University. This Biobank operates under the administration of the Human Tissue and Cell Research (HTCR) Foundation. The framework of HTCR Foundation (Thasler et al., 2003), which includes obtaining written informed consent from all donors, has been approved by the ethics commission of the Faculty of Medicine at the Ludwig-Maximilians University (approval number 025-12) as well as the Bavarian State Medical Association (approval number 11142) in Germany. Experimental procedures were performed in accordance with the Declaration of Helsinki. Donor data are shown in Supplemental Table 1. Primary human hepatocytes were isolated by the Biobank using a two-step collagenase perfusion technique with modifications (Lee et al., 2013). The cells were cultivated and treated with chemicals as described before (Jeske et al., 2017).

RNA Isolation and Reverse-Transcription Quantitative Real-Time PCR Analysis. Total RNA was isolated using the NucleoSpin RNA kit (Machery-Nagel, Düren, Germany), including on-column DNase I digest. RNA integrity was analyzed by formaldehyde-agarose gel electrophoresis. cDNA was synthesized as described previously (Jeske et al., 2017).

Relative quantification analyses ($\Delta\Delta C_t$) were performed in technical triplicates by TaqMan RT-qPCR using the BioMark HD system and 48.48 Dynamic Array or Flex Six Gene Expression Integrated Fluidic Circuits (Fluidigm, South San Francisco, CA), as described previously (Jeske et al., 2017). The following TaqMan gene expression assays (Life Technologies) were used: Hs00184500_m1 (ABCB1), Hs01546975_gH (AKR1B10), Hs00946140_g1 (CYP2C8), Hs00604506_m1 (CYP3A4), Hs01005622_m1 (FASN), Hs00378308_m1 (SMPDL3A), and Hs99999902_m1 (RPLP0). The CYP2B6, EPHX1, and UGT1A3 assays have been described previously (Burk et al., 2005; Riedmaier et al., 2010; Hoffart et al., 2012). Data were analyzed as described before (Jeske et al., 2017), and gene expression levels were normalized to corresponding 18S rRNA levels as determined using the 18S rRNA assay previously described (Hoffart et al., 2012). Serial dilutions of respective linearized cDNA plasmids, which were treated just as cDNA samples, were used to determine linearity of the assays (between 375,000 and 37.5 copies).

Experimental Design and Data Analyses. All experiments were done in an exploratory manner. Thus, *P* values have to be interpreted as descriptive only. The decision to perform five independent experiments (except competitive PXR binding and hepatocyte experiments) was made prior to their execution based on the level of variation observed in previous work. In Fig. 4, A, C and D, the number of independent experiments for controls (RIF, without NFV, or without M8) exceeds five because of technical reasons. To avoid systematic errors due to timing and/or positioning in limited proteolytic digestion and transfection experiments, the sequence of chemical treatment of cells and measurement of samples was randomized for independent experiments.

Experimental data are shown in scatter plots with mean ± S.D. or medians with interquartile ranges of at least five independent experiments. Numbers of independent experiments are presented in the respective figure legends. Medians were used only with primary human hepatocytes, as independent experiments were performed here with cultures from different donors. Statistical comparisons were performed with repeated-measures one-way or two-way ANOVA or Friedman test using respective post hoc tests for multiple comparisons against specified controls as recommended by the analysis software and described in the figure legends. Comparisons to a hypothetical value were performed with one sample *t* test or Wilcoxon signed rank test for means or medians, respectively. Pairwise comparisons of medians were performed with Wilcoxon matched-pairs signed rank test. EC_{50} and IC_{50} values were determined by nonlinear fit of concentration response using the equation for sigmoidal dose response [log agonist or log inhibitor vs. response (three parameters)]. All calculations were done with GraphPad Prism 8.4.2 (GraphPad Software, San Diego, CA).

Results

Nelfinavir and Its Metabolite M8 Modulate the Activities of PXR and Further Nuclear Receptors. Expression of drug-metabolizing enzymes and transporters is not exclusively induced via PXR but also by further ligand-activated nuclear receptors [for a review, see Pascussi et al. (2003); Prakash et al. (2015)]. Thus, we investigated whether nelfinavir and its metabolite M8 (Fig. 1A) modulate the activities of respectively selected nuclear receptors using the corresponding promoter reporter gene assays in agonist (Fig. 1B) and antagonist (Fig. 1C) modes. To determine the applicable concentration, the effects of increasing concentrations of the compounds on viability of HepG2 cells were analyzed. Supplemental Fig. 1 shows for both compounds that concentrations exceeding 10 μM resulted in HepG2 viability of less than 80%. Thus, single concentration of 10 μM of nelfinavir and M8 was selected for starting analyses. In accordance with published results (Svärd et al., 2010; Lynch et al., 2015), nelfinavir induced PXR activity by 3.7-fold (95% CI 3.1–4.3-fold) while inhibiting the constitutive activity of CAR1 by 60% (95% CI 51%–72%). In addition, FXRα2 was also activated 2.0-fold (95% CI 1.7–2.3-fold) by nelfinavir. M8 selectively induced PXR activity by 5.1-fold (95% CI 4.5–5.7-fold) (Fig. 1B). The 20% reduction of basal PPARγ1 activity may indicate antagonism of M8. Figure 1C shows that nelfinavir antagonized rifampin-dependent PXR activity by 35% (95% CI 19%–51%), whereas M8 demonstrated 50% (95% CI 24%–77%) inhibition. Ligand-activated VDR was inhibited by 15% or 45% in the presence of nelfinavir or M8, respectively, whereas the activity of GW4064-induced FXRα2 was reduced by 17% or 40%, respectively. In addition, the activities of ligand-activated CAR3, LXRβ, and PPARγ1 were all reduced by approximately 30% in the presence of M8.

To corroborate the above-described effects of nelfinavir and M8 on nuclear receptors besides PXR, respective concentration-response analyses were conducted. Nelfinavir-dependent inhibition of CAR1 and activation of FXRα2 were confirmed unequivocally (Supplemental Fig. 2, A and E). However, the effects on the other nuclear receptors, which mainly consisted of slight inhibition of agonist-induced receptor activities by M8, were exclusively obtained with 10 μM. Concentration-dependent effects, as with CAR1 and FXRα2, were not observed (Supplemental Fig. 2, B–D, F–H). Given the sharp decline in viability of HepG2 between 10 and 30 μM of M8 (Supplemental Fig. 1), it cannot be excluded that the effects observed with 10 μM M8 stemmed from partial cytotoxicity. In conclusion, nelfinavir and its metabolite M8 not only activated PXR but also antagonized the ligand-activated receptor. Additionally,

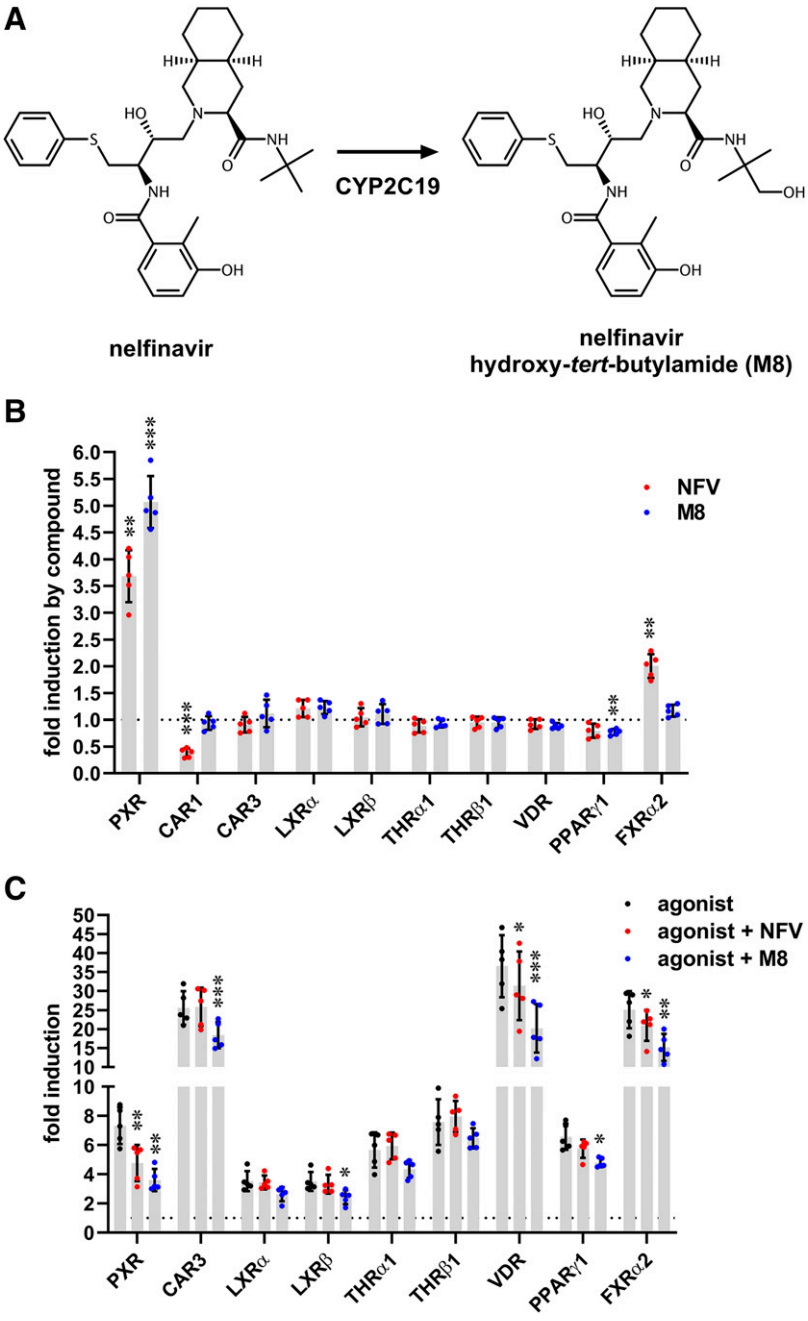

Fig. 1. Effects of nelfinavir and M8 on nuclear receptor activities. (A) Chemical structures of nelfinavir and its active metabolite M8 generated by CYP2C19. (B and C) HepG2 cells were cotransfected with expression plasmids encoding the indicated nuclear receptors and corresponding reporter gene plasmids, as specified in *Materials and Methods*. Chemical treatments lasted for 24 hours. (B) Transfected cells were treated with 0.1% DMSO or 10 μM NFV or M8. Data are shown as scatter plots with mean (columns) fold induction ± S.D. (n = 5) of normalized luciferase activities of the respective reporter genes by chemical treatment, as compared with the corresponding treatments with vehicle DMSO only, which were each designated as 1. Differences to this value were analyzed by one sample t test, and P values were corrected for multiple testing by the method of Bonferroni. (C) Transfected cells were treated with 0.1% DMSO or corresponding prototypical nuclear receptor agonists as specified in *Materials and Methods*, with or without 10 μM NFV or M8. Data are presented as shown above, with mean ± S.D. (n = 5). Differences to treatments with respective agonists only were analyzed by repeated-measures one-way ANOVA with Dunnett's multiple comparisons test. $^{*}P < 0.05$; $^{**}P < 0.01$; $^{***}P < 0.001$. THR, thyroid hormone receptor.

nelfinavir inhibited CAR1 and activated FXRα2, whereas effects on some other nuclear receptors, especially by M8, have to be regarded as uncertain because of the possibility of partial cytotoxicity.

Direct Binding of Nelfinavir and M8 to PXR. As mentioned above, activation of PXR by nelfinavir and M8 may be explained theoretically by the inhibition of inhibitory protein kinases. However, the antagonistic effects on rifampin-induced PXR activity identified here call for a different explanation. Thus, direct binding of the compounds to PXR was reinvestigated. First, we addressed binding by in silico molecular docking of nelfinavir and M8 into different potential binding sites. An ensemble docking approach was chosen by which nelfinavir and M8 were flexibly docked into the LBP and AF-2 groove of six different PXR X-ray crystal structures. Docking scores of the top-ranked poses of both compounds were similar for the LBP (107.4 for nelfinavir vs. 110.4 for M8) and thus do not indicate a preferred binding of either nelfinavir or M8 over the other. Docking scores for the AF-2 groove were substantially lower (nelfinavir: 84.2; M8: 85.4), indicating a preference of both compounds for the LBP (Supplemental Table 2). To evaluate binding of nelfinavir and M8 to alternative sites on the LBD, an in silico approach for pocket detection was employed (Fig. 2A). Only pockets with either a size of >50 alpha spheres or a calculated propensity for ligand binding >1 were considered, resulting in a total of eight potential alternative binding sites (Fig. 2A; Supplemental Table 2) into which nelfinavir and M8 were docked. Docking scores for all alternative sites were substantially lower compared with the scores obtained for the

LBP (63.7–82.9). Thus, the further analysis was continued only for nelfinavir and M8 docking poses within the LBP. Clustering of the docking poses revealed the ten top-ranked poses (RMS deviation cut-off: 1.5 Å) of nelfinavir to appear in two clusters and two single conformations (Supplemental Table 3). Six of the ten best-scored docking poses belong to the same cluster. In contrast, the ten top-ranked conformations for M8 grouped into five clusters and one single conformation. The visualization of the top-ranked docking poses of each cluster showed that M8 samples a considerably larger conformational space in the LBP compared with nelfinavir (Fig. 2, B and C). This suggests the preference of nelfinavir for a specific binding mode within the LBP compared with M8.

The in silico prediction of binding was checked experimentally with the limited proteolytic digestion assay. Figure 3A shows that nelfinavir as well as its metabolite M8 result in concentration-dependent increase in protection of three main proteolytic fragments of the 36 kDa PXR-LBD protein from trypsin digestion. At the highest concentration, nelfinavir showed 5.3-fold increase (95% CI 3.7–7.0-fold), whereas M8 showed 5.4-fold increase (95% CI 4.5–6.2-fold). Similarly, the high-affinity PXR ligand T0901317 demonstrated 5.0-fold increase (95% CI 4.3–5.7-fold). T0901317 protected the same main proteolytic fragments, although to varying extents. Although nelfinavir and M8 only weakly protected the 26-kDa fragment, T0901317 efficiently protected all three, suggesting that PXR binding of nelfinavir and M8 may have resulted in an LBD conformational change different from that generated by binding of T0901317. To further confirm direct binding to PXR, a competitive PXR binding assay was deployed (Fig. 3B). EC_{50} value of percentage relative binding of positive control SR12813 was determined as 45.6 nM (95% CI 22.7–94.1 nM), which is in line with published data (Dong et al., 2010). Nelfinavir and M8 also demonstrated PXR binding in this assay with EC_{50} values of 89.0 nM (95% CI 48.2–167 nM) and 51.1 nM (95% CI 18.7–148 nM), respectively. In summary, these data provide evidence for direct binding of nelfinavir and M8 to the PXR-LBD.

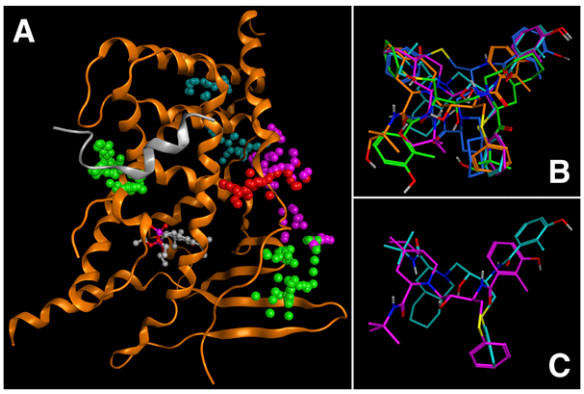

Fig. 2. In silico analysis of nelfinavir and M8 binding to PXR. (A) Location of alternative binding sites, indicated by colored alpha spheres (1M13, green: 1NRL:A, cyan; 1NRL:B, magenta; 2O9I:A, red) on the PXR-LBD (orange ribbon). The steroid receptor coactivator-1 peptide indicating the location of the AF-2 groove is shown as gray ribbon. The LBP-bound ligand SR12813 is shown as ball-and-stick representation with carbon atoms in gray. Comparison of the binding modes of (B) M8 and (C) nelfinavir docked into the PXR-LBP. Different colors indicate the top-ranked conformation of each cluster using a RMS deviation cut-off of 1.5 Å.

Nelfinavir and M8 Are Partial Agonists of PXR that Also Act as Competitive Antagonists. Having established ligand binding to PXR, further characterization of the respective activation and inhibition properties of nelfinavir and M8 called for cellular concentration-response analyses. Respective analyses were performed with H-P cells, a HepG2 clone stably expressing PXR (Bitter et al., 2015). Similar to parental HepG2 cells, H-P cells showed decreased viability at compound concentrations exceeding 10 μM; however, they were not as sensitive toward M8 as HepG2 (Supplemental Fig 1). Figure 4A shows that the agonist efficacies of nelfinavir and M8 were reduced if compared with rifampin. At 10 μM, the two compounds exhibited only 30%–40% of the activity seen by the same concentration of rifampin, thereby indicating partial agonism. Keeping in mind that the M8 concentration-response curve did not yet approximate plateau, nelfinavir demonstrated EC_{50} of 0.9 μM (95% CI 0.58–1.3 μM), whereas M8 showed reduced potency with EC_{50} of 7.5 μM (95% CI 4.4–14.9 μM). Using the same assay, rifampin EC_{50} of 2.4 μM (95% CI 1.6–3.6 μM) proved to be elevated compared with previously reported EC_{50} values of 1.3 and 1.8 μM (Lin et al., 2008; Hoffart et al., 2012). Partial agonism was also observed for nelfinavir-dependent activation of a GAL4-DBD/PXR-LBD fusion protein (Supplemental Fig. 3). Cotreatment with the specific PXR antagonist SPA70 (Lin et al., 2017) almost completely suppressed the reporter activation by nelfinavir and M8 (Fig. 4B), thereby testifying to PXR dependency. Competitive antagonism of the compounds was observed when rifampin concentration-response curves were established in the presence of increasing concentrations of nelfinavir (Fig. 4C) or M8 (Fig. 4D). In both cases, rifampin concentration-response curves were shifted to the right, and respective EC_{50} values increased with elevated concentrations of the antagonistic compounds (Supplemental Table 4). Analysis of the increase in rifampin EC_{50} values revealed statistical significance only for 10 μM nelfinavir. However, a respective trend was observed for 3 μM nelfinavir and 10 μM M8 (Fig. 4E). IC_{50} values of nelfinavir and M8 antagonism were determined for the inhibition of PXR activation by 10 μM rifampin (Fig. 4F). With IC_{50} of 7.3 μM (95% CI 5.0–11.0 μM), nelfinavir proved to be the more potent antagonist when compared with M8 with its IC_{50} of 25.3 μM (95% CI 16.1–47.2 μM). Nelfinavir further proved to antagonize PXR activation by the high-affinity ligand T0901317 (Supplemental Fig. 4). Because nelfinavir and M8 comparably affected PXR, and cytotoxicity of M8 was more pronounced, further investigations were performed only with the parent drug.

Competitive Antagonism of Nelfinavir Exclusively Depends on Binding into the PXR Ligand-Binding Pocket. Since the concentration of nelfinavir had to be restricted to 10 μM, additional allosteric antagonism at higher concentrations, as observed for the PXR mixed competitive/noncompetitive allosteric antagonist pimecrolimus (Burk et al., 2018), may have remained undetected. Thus, we investigated the ability of nelfinavir to inhibit the constitutive activity of a PXR mutant with the LBP filled with bulky amino acid residues. Such a mutant is no longer activated by agonists because these cannot bind into the LBP (Wang et al., 2008), but its constitutive activity can be antagonized by compounds exclusively or additionally binding outside of the LBP (e.g., coumestrol, pazopanib, or pimecrolimus) (Wang et al., 2008;

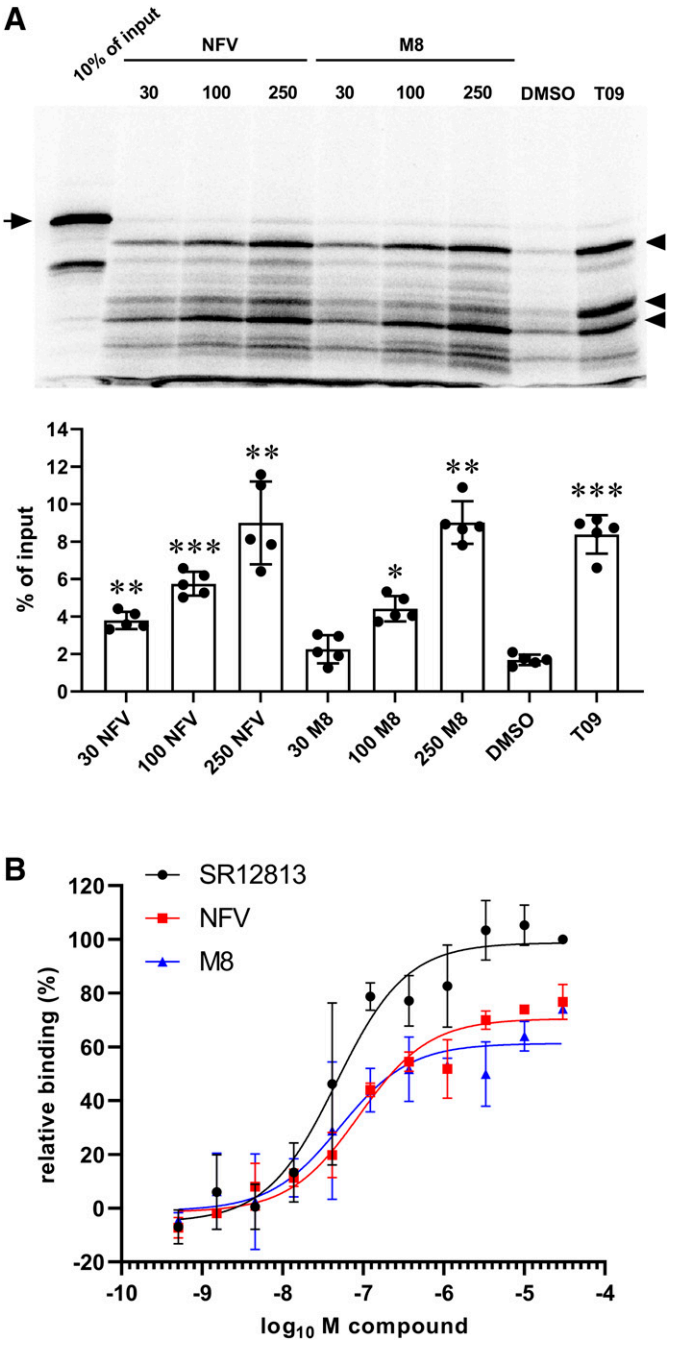

Fig. 3. Analysis of in vitro binding of nelfinavir and M8 to PXR-LBD. (A) Limited proteolytic digestion analysis of PXR-LBD protein, which was incubated with 30, 100, or 250 μM NFV or M8, 30 μM T0901317 (T09), or 2.5% DMSO. Upper panel shows the radioluminographic scan of a representative experiment with 36 kDa undigested input protein (arrow) and protected proteolytic fragments of 32, 26, and 23 kDa (arrow heads). Lower panel shows the respective densitometric quantifications of the sum of the three protected fragments, calculated as percent of input. Data are presented as scatter plots with mean (columns) ± S.D. ($n = 5$). Differences to incubation with vehicle DMSO only were analyzed by repeated-measures one-way ANOVA with Dunnett's multiple comparisons test. $^{*}P < 0.05$; $^{**}P < 0.01$; $^{***}P < 0.001$. (B) Competitive ligand binding to the PXR-LBD using the LanthaScreen TR-FRET kit. Concentration-dependent response is shown for the indicated compounds between 0.5 nM and 30 μM as mean of relative binding (%) ± S.D. from two independent experiments, with each done in technical triplicates. Relative binding was calculated as described in *Materials and Methods*. Two-percent DMSO was used as negative control, and 30 μM SR12813 was used as positive control (100% relative binding).

Burk et al., 2018). Accordingly, nelfinavir showed activation of wild-type PXR but not of the LBP-filled triple mutant S208W/S247W/C284W, which is similar to the prototypical PXR agonist rifampin. Nelfinavir, which inhibited the rifampin-dependent activation of wild-type PXR by 54% (95% CI 29%–80%), did not antagonize the high constitutive activity of the mutant (Fig. 5), thereby indicating that it has to bind to the LBP to exhibit its inhibitory effect.

Impaired Coactivator Recruitment Accounts for the Effects of Nelfinavir on PXR Activation. To characterize the functional consequences of nelfinavir interaction with PXR, cellular mammalian two-hybrid assays were performed, which address ligand-dependent LBD assembly, corepressor release, and coactivator recruitment. In clear contrast with the partial agonism of nelfinavir in the CYP3A4 enhancer/promoter reporter gene assay (as shown in Fig. 4A), the drug induced the PXR-LBD assembly more strongly (mean increase by 70%, 95% CI 19%–120%) than rifampin (Fig. 6A). The constitutive interaction of PXR with corepressor NCOR2 in the absence of ligand was diminished by nelfinavir to a similar extent as by rifampin (Fig. 6B). In the established sequence of events during nuclear receptor activation, recruitment of coactivators follows the ligand-dependent release of corepressors. Whereas rifampin induced the interaction of PXR with coactivators NCOA1, NCOA2, and MED1 by 8-fold (95% CI 4.6–12.2-fold), 9.3-fold (95% CI 7.3–11.3-fold), and 4.6-fold (95% CI 3.9–5.4-fold), respectively, nelfinavir demonstrated impaired recruitment for all coactivators, which have been tested (Fig. 6, C–E). Furthermore, nelfinavir reduced the rifampin-dependent recruitment of NCOA1 to 3.2-fold (95% CI 1.8–4.6-fold) in cotreatment (Fig. 6C). Similar effects were observed with NCOA2 (4.1-fold, 95% CI 3.5–4.7-fold) (Fig. 6D) and MED1 (2.2-fold; 95% CI 2.0–2.4-fold) (Fig. 6E). Taken together, these data indicate that the partial agonism and competitive antagonism of nelfinavir in PXR activation depend on the impaired recruitment of coactivators. Corepressor release and intramolecular conformational changes in response to ligand binding, the latter as described by the LBD assembly assay, are not compromised.

Nelfinavir Differentially Induces PXR Target Genes in Primary Human Hepatocytes and Antagonizes Rifampin Induction. Given the weak activation of PXR by nelfinavir in reporter gene assays, the question arises: To what extent may the compound be able to induce the expression of endogenous PXR target genes? Primary human hepatocytes, which were treated with nelfinavir, demonstrated induction of only a subset of selected PXR-regulated genes as compared with treatment with rifampin. Cytochrome P450 genes, such as CYP2B6, CYP2C8, and CYP3A4, which proved to be highly inducible by rifampin, also demonstrated induction by nelfinavir. Nelfinavir further induced the expression of EPHX1 and UGT1A3. However, genes, such as ABCB1, AKR1B10, FASN, or SMPDL3A, which showed weak to moderate induction by rifampin, were not induced by nelfinavir (Fig. 7A). Among the genes induced by both compounds, UGT1A3 was the only one that showed no difference in induction by rifampin and nelfinavir. Neither rifampin nor nelfinavir induced the expression of RPLP0, which is not a target gene of PXR.

Figure 7B shows that cotreatment with increasing concentrations of nelfinavir antagonized the induction of ABCB1 and CYP3A4 by rifampin, whereas the respective effect was not

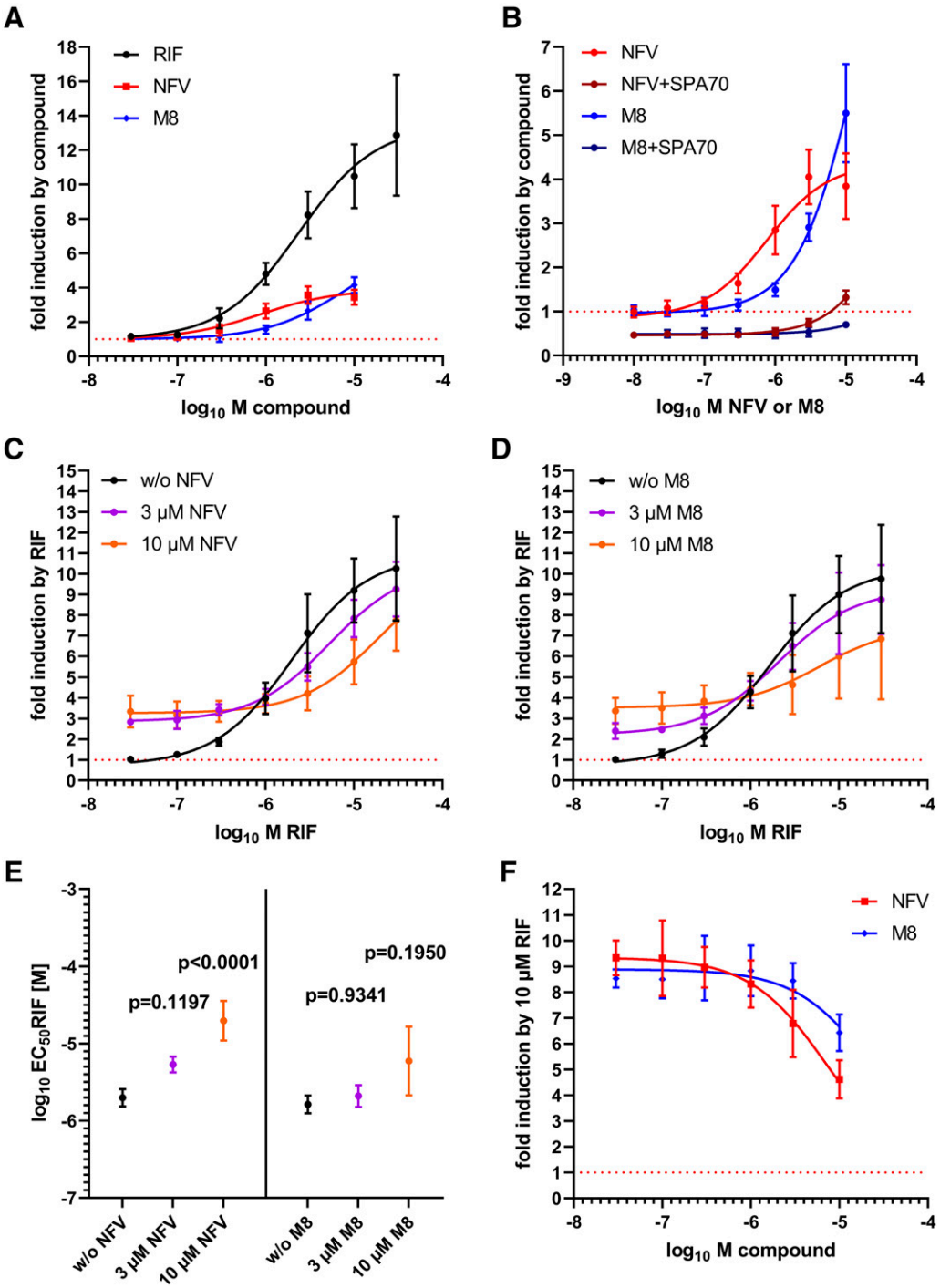

Fig. 4. Concentration-dependent response of PXR activation by nelfinavir and M8 and antagonistic effects on activation by rifampin. H-P cells were transfected with CYP3A4 reporter and (A) treated for 24 hours with increasing concentrations of RIF, NFV, or M8; (B) treated with increasing concentrations of nelfinavir or M8 in the presence or absence of 3 μM SPA70; (C and D) cotreated with increasing concentrations of rifampin in the presence of the indicated fixed concentrations of (C) nelfinavir or (D) M8; and (F) cotreated with increasing concentrations of nelfinavir or M8 in the presence of 10 μM rifampin. Mean fold induction ± S.D. ($n \geq 5$) by the respective treatment is shown with respect to the normalized reporter activity of cells treated with vehicle DMSO only, which was designated as 1. Nonlinear fit of concentration-dependent response was performed with bottom values fixed to 1 in (A and F). (E) shows the mean ± S.E. of rifampin $\log_{10}$ EC_{50} values derived from experiments shown in (C and D) ($n = 5$), which have been calculated as described in *Materials and Methods*. Differences to rifampin $\log_{10}$ EC_{50} values in the absence of nelfinavir or M8 were analyzed by one-way ANOVA with Dunnett's multiple comparisons test according to GraphPad Prism knowledgebase article 144 (GraphPad Software, accessed August 17, 2020, https://www.graphpad.com/support/faq/how-can-i-test-for-differences-among-three-or-more-curves-fitted-to-three-or-more-data-sets/). w/o, without.

statistically significant for CYP2B6, most likely because of the high variability of CYP2B6 induction by rifampin in this experimental set of hepatocytes. Interestingly, treating the cells with 30 μM nelfinavir only did not result in stronger induction of the genes as compared with 10 μM. In the case of CYP3A4, induction even appeared to be suppressed.

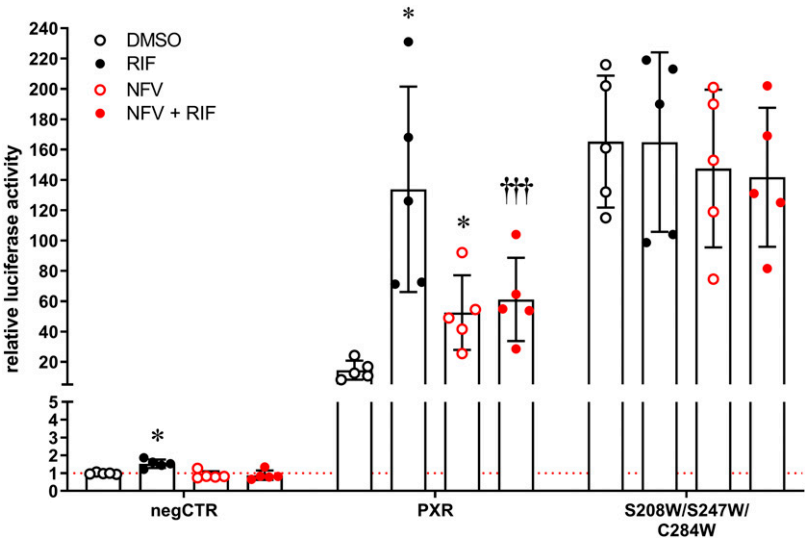

Fig. 5. Analysis of the effect of nelfinavir on LBP-filled PXR mutant. HepG2 cells were transfected with empty expression vector pcDNA3 (negCTR) or expression plasmids encoding wild-type PXR or the LBP-filled triple PXR mutant S208W/S247W/C284W and treated for 24 hours with 0.1% DMSO or 10 μM NFV with or without 10 μM RIF. Normalized luciferase activities of cotransfected CYP3A4 reporter are presented in scatter plots with mean (columns) ± S.D. ($n = 5$) relative to the activity of cells transfected with pcDNA3 and treated with DMSO only. Differences to respective treatments with DMSO (asterisks, exclusively for single-compound treatments) or with rifampin only (daggers, exclusively for nelfinavir + rifampin cotreatment) were analyzed by repeated-measures two-way ANOVA with Dunnett's or Sidak's multiple comparisons tests, respectively. *$P < 0.05$; †††$P < 0.001$.

Discussion

We have characterized here in detail the interaction of the HIV protease inhibitor nelfinavir and its major metabolite M8 with PXR. Both compounds act as partial agonists and competitive antagonists of human PXR by binding into the LBP of the receptor. The partial agonist/antagonist properties mainly result from impaired coactivator recruitment.

Nelfinavir and its major metabolite M8, which accounts for 80%–90% of primary metabolites detected in human plasma (Zhang et al., 2001), exert the same functional effects on PXR, and thus it is not expected that hepatic metabolism of the drug may limit modulation of the receptor. M8 selectively activated PXR, whereas nelfinavir also induced the activity of FXR and, as already reported (Lynch et al., 2015), inhibited CAR. In the antagonist mode, slight inhibition of the ligand-dependent activation of several other nuclear receptors by 10 μM M8 was observed (see Fig. 1C and Supplemental Fig. 2), which, however, cannot be excluded to result from partial cytotoxicity. Even if the inhibition by 10 μM M8 would reflect true antagonism of the activity of these nuclear receptors, the biologic relevance of such small effects is still questionable.

Direct binding of nelfinavir and M8 to PXR was suggested by docking into the LBP of the receptor's X-ray crystal structures. Neither the AF-2 groove nor any of the identified potential alternative binding sites seem to be suited to favorably bind any of both compounds. Binding of nelfinavir to the LBP appeared to be more favorable compared with M8 because nelfinavir showed a clear preference for a specific binding mode. This may explain the lower EC_{50} and IC_{50} values determined for the parent drug. Because nelfinavir is a more hydrophobic compound (logP: 4.7) compared with M8 (logP: 3.7), nelfinavir binding to the largely hydrophobic PXR-LBP might be more favorable.

The limited proteolytic digestion and TR-FRET–based competitive ligand-binding assays performed here showed for the first time experimental evidence that nelfinavir and its metabolite M8 bind to the LBD of PXR. Using a radioligand-binding competition assay, Dussault et al. (2001) failed to demonstrate binding of nelfinavir to PXR. Nevertheless, mean inhibition by 20%–25% is visible in the respective data, which the authors regarded as irrelevant. It may be argued that protection from digestion by trypsin is simply reflecting direct protease inhibition by nelfinavir and its metabolite. However, omitting the ligand preincubation step in the limited proteolytic digestion experiment and only adding the compounds together with trypsin resulted in a strong decrease in protection of PXR from digestion by the protease. The residual protection is most likely due to ligand binding during the coincubation with trypsin, as it was likewise observed with T0901317 (unpublished data). Accordingly, it has been reported that nelfinavir does not inhibit trypsin activity (Wignot et al., 2004; Singh et al., 2009). The result of the limited proteolytic digestion assay was confirmed by the TR-FRET–based PXR ligand-binding competition assay, which further demonstrated nelfinavir and M8 EC_{50} values for binding to the PXR-LBD comparable with respective EC_{50} of the potent PXR agonist SR12813. Ligand binding of nelfinavir and M8 does not necessarily disqualify an indirect activation mechanism by the inhibition of protein kinases. This mechanism may additionally contribute to activation of PXR by nelfinavir and may further limit nelfinavir-dependent antagonism. Final proof that kinase inhibition contributed to nelfinavir-dependent PXR modulation awaits the analysis of PXR protein phosphorylation after treatment with the drug.

EC_{50} value in the range of 0.1 μM for in vitro binding to PXR indicates physiologic relevance of the modulation of PXR activity by nelfinavir. The drug shows extremely high intracellular accumulation (Jones et al., 2001; Mateus et al., 2017). Treatment of lymphoblastoid CEM cells with 10 μM nelfinavir for 18 hours resulted in intracellular concentration of approximately 700 μM (Jones et al., 2001). Since the fraction of unbound intracellular nelfinavir was determined in different cell lines to range from 0.0001 to 0.0004 (Mateus et al., 2017), unbound intracellular concentration can be roughly estimated to range from 0.1 to 0.3 μM, which can be expected as sufficient for PXR activity modulation. Furthermore, dosing mice with nelfinavir in a way that resulted in similar blood concentrations as the therapeutic dosing of patients with HIV subsequently produced amounts in liver, which corresponded to intracellular amounts in HeLa cells treated with 5–10 μM nelfinavir for 6 hours (de Gassart et al., 2016). These data provide indirect evidence that the intracellular concentrations of nelfinavir, which were achieved by

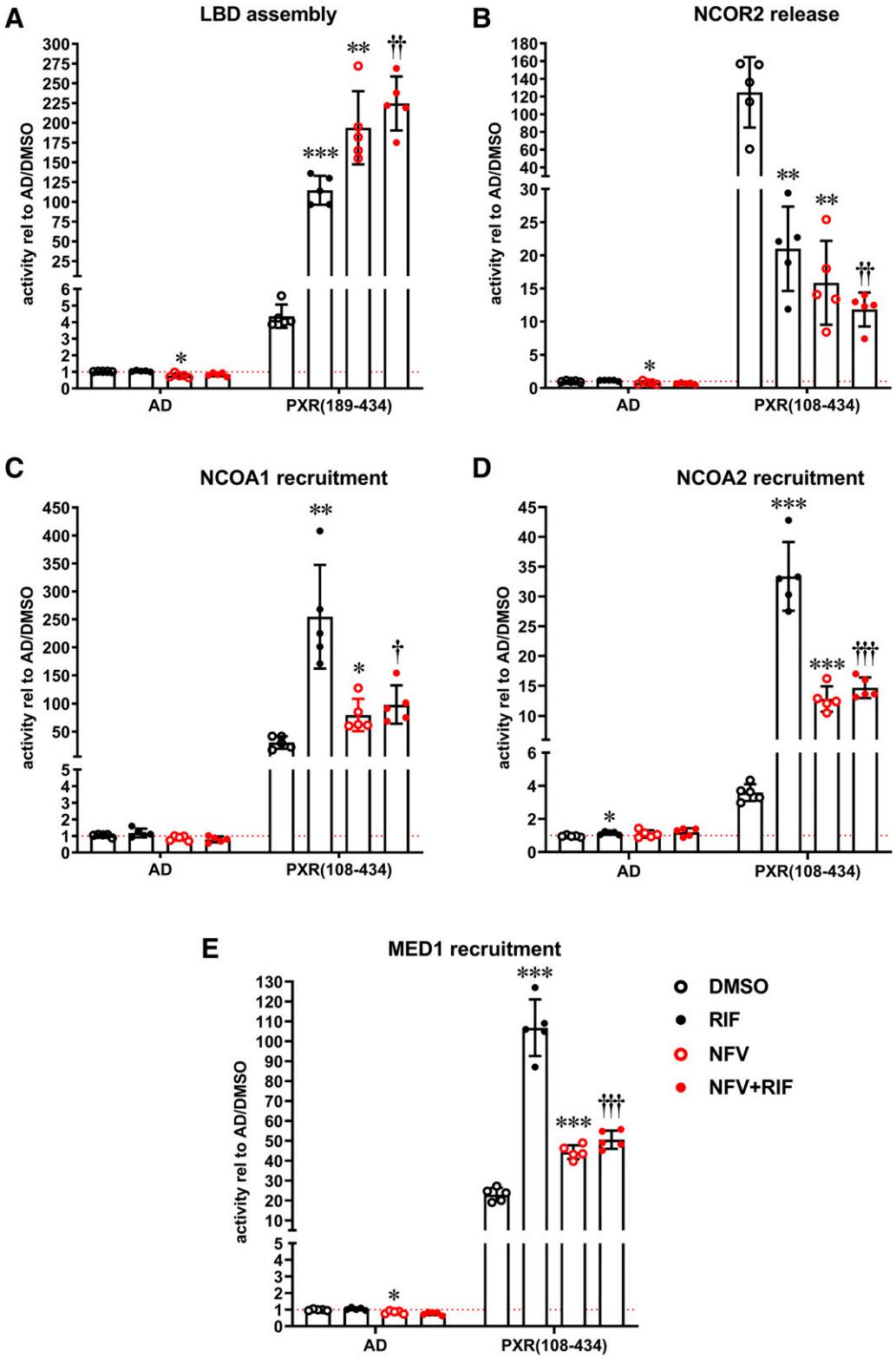

Fig. 6. Effects of nelfinavir on PXR-LBD assembly and transcriptional cofactor interaction. (A) HepG2 cells were cotransfected with combinations of expression plasmids encoding GAL4-DBD/PXR-LBD (132–188) and VP16-AD/PXR-LBD (189–434) or empty vector pVP16-AD. (B–E) HepG2 cells were cotransfected with expression plasmids encoding VP16-AD/PXR-LBD (108–434) fusion protein or empty vector pVP16-AD and expression plasmids encoding fusion proteins of (B) GAL4-DBD/NCOR2-RID, (C) GAL4-DBD/NCOA1-RID, (D) GAL4-DBD/NCOA2-RID, or (E) GAL4-DBD/MED1-RID. Transfected cells were treated with 0.1% DMSO or 10 μM NFV with or without 10 μM RIF for 24 hours. Data are presented as scatter plots with mean (columns) ± S.D. ($n = 5$) of normalized luciferase activity of the cotransfected pGL3-G5 relative to the activity of cells transfected with pVP16-AD and treated with DMSO only. Differences to respective treatments with DMSO (asterisks, exclusively for single-compound treatments) or with rifampin only (daggers, exclusively for nelfinavir + rifampin cotreatment) were analyzed by repeated-measures two-way ANOVA with Dunnett's or Sidak's multiple comparisons tests, respectively. *†$P < 0.05$; **††$P < 0.01$; ***†††$P < 0.001$.

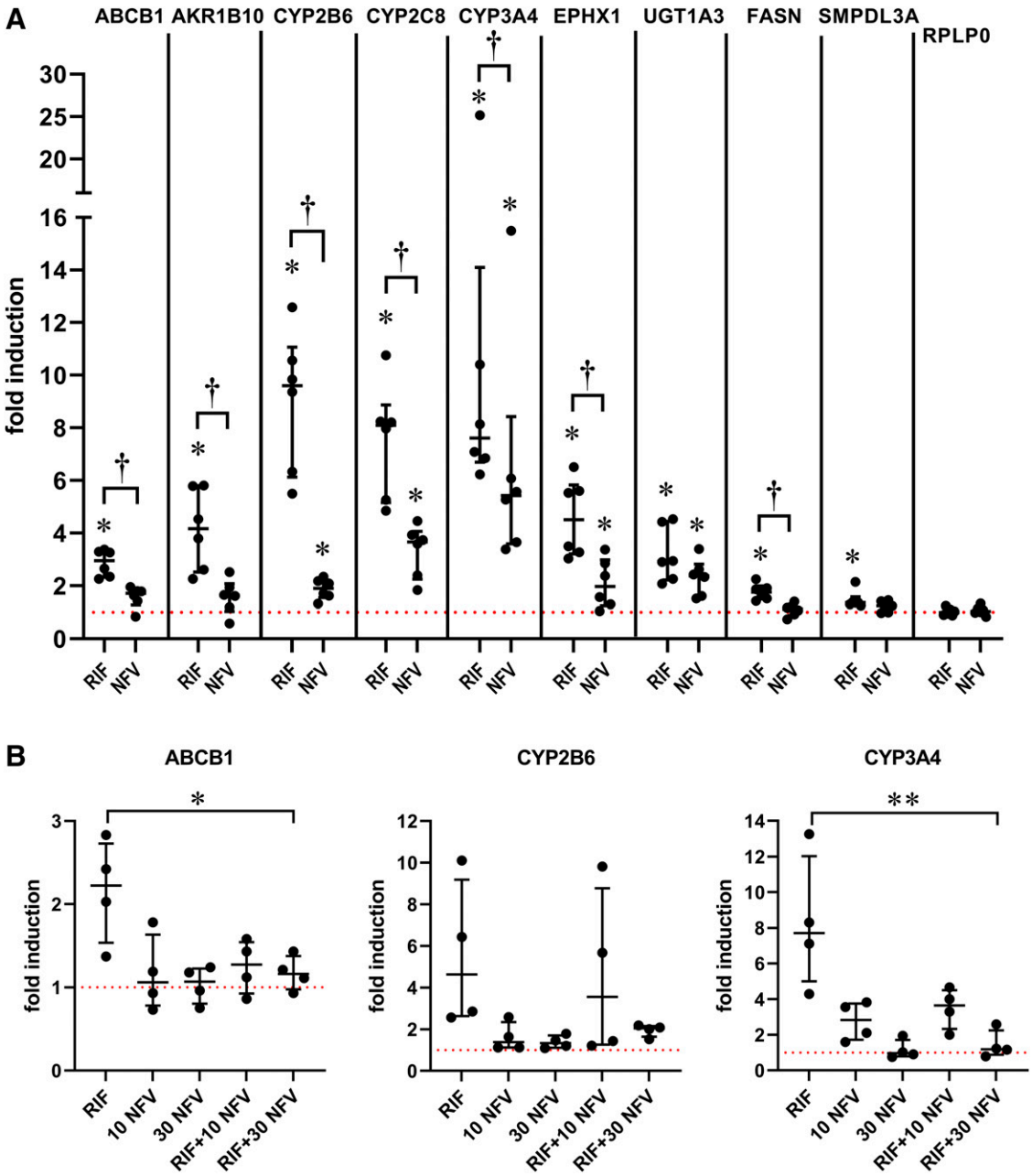

Fig. 7. Effects of nelfinavir on the expression of endogenous PXR target genes in hepatocytes. (A) Cultures of primary human hepatocytes of six donors were each treated with 0.1% DMSO, 10 μM RIF, or 10 μM NFV for 24 hours. mRNA expression of the indicated genes was determined by TaqMan RT-qPCR and normalized to the expression of 18S rRNA. Data are presented in scatter plots with medians and interquartile ranges. Expression was calculated as fold induction caused by the respective chemical treatment as compared with the expression in cells treated with vehicle DMSO only, which was designated as 1. Differences to this value were analyzed by one sample Wilcoxon signed rank tests (asterisks). Differences between rifampin and nelfinavir treatments were analyzed by Wilcoxon matched-pairs signed rank tests for each gene individually (daggers). (B) Cultured primary human hepatocytes of four donors were treated for 24 hours with 0.1% DMSO or 10 or 30 μM NFV in the absence or presence of 10 μM RIF. mRNA expression of the indicated genes was calculated and is presented as described above. Differences to treatment with rifampin only were analyzed by Friedman test with Dunn's multiple comparisons test (asterisks, exclusively for cotreatments of rifampin and nelfinavir). *,†$P < 0.05$; **$P < 0.01$.

treatment of cells with 10 μM of the compound in the culture medium, thereby exerting PXR-dependent effects, can be expected in vivo in the liver by therapeutic dosing. Physiologic relevance is further supported by induction of endogenous gene expression in primary human hepatocytes by 10 μM nelfinavir (see Fig. 7A). Nelfinavir may have demonstrated gene-specific induction, as only part of the genes, which have been analyzed, were induced by the drug. These include CYP2B6, CYP2C8, CYP3A4, EPHX1, and UGT1A3, whereas ABCB1, AKR1B10, FASN, and SMPDL3A were not induced. Missing induction of ABCB1 is in contrast with previous reports, which demonstrated induction of the gene (Dixit et al., 2007, Liu et al., 2012). The difference may be explained by donor-dependent gene expression variability of primary human hepatocytes.

Nelfinavir was proven here to act as both a partial agonist and a competitive antagonist of PXR, inhibiting activation by pure agonists, such as rifampin and T0901317, in hepatic

cells. These characteristics are mainly due to the impaired recruitment of coactivators, whereas corepressor release is not compromised as compared with a full agonist. In this respect, nelfinavir equals partial agonists of PPARγ, such as GW0072, FK614, or PA-082 (Oberfield et al., 1999; Fujimura et al., 2005; Burgermeister et al., 2006), which were proven to be selective receptor modulators. In CV-1 cells, nelfinavir neither activated a fusion protein of the GAL4-DBD with the PXR-LBD nor resulted in recruitment of coactivator MED1 (Dussault et al., 2001). This may indicate cell-type specificity and thus selective receptor modulation. Failure of PXR activation in CV-1 cells was not simply due to the use of a GAL4-DBD/PXR-LBD fusion protein. Performing an equivalent experiment in HepG2 cells resulted in the same partial agonism of nelfinavir (Supplemental Fig. 3) as observed with full-length PXR in CYP3A4 reporter assays. Nelfinavir may thus be regarded as a basic structure for the development of specific PXR-selective receptor modulators. However, this would require detailed information on the binding mode of nelfinavir in the PXR-LBP, which clearly requires the elucidation of the nelfinavir-bound PXR crystal structure.

We have shown here that nelfinavir competitively antagonized PXR activity, which may be of physiologic relevance because the drug also antagonized PXR-dependent induction of ABCB1 and CYP3A4 in hepatocytes (see Fig. 7B). PXR antagonism by nelfinavir may contribute further to the nelfinavir-dependent resensitization of cancer cells to cytotoxic drug treatment (Kim et al., 2019). This applies particularly in the case that the development of chemoresistance involved PXR activation. Several anticancer drugs, such as paclitaxel and cisplatin (Masuyama et al., 2005), vincristine and vinblastine (Harmsen et al., 2010), SN-38, the active metabolite of irinotecan (Basseville et al., 2011), and sorafenib (Feng et al., 2018), were shown to bind to and/or activate PXR. Chemoresistance generated by treatment with these drugs may thus have been caused by PXR activation (Planque et al., 2016; Feng et al., 2018). Consequently, PXR antagonists may resensitize chemoresistant cancer cells. This concept was recently validated by the resensitization of cisplatin-resistant HepG2 cells by treatment with the PXR antagonist leflunomide (Yasuda et al., 2019). However, the PXR-dependent effects of nelfinavir in cancer cells and especially in chemoresistant cancer cells require further study.

Modulation of PXR by nelfinavir may not necessarily result in anticancer activity. In models of breast, prostate, or colorectal cancer, PXR induces tumor progression and chemoresistance (Pondugula et al., 2016). If PXR has not yet been activated in such a context, treatment with nelfinavir may activate the receptor and counteract nelfinavir-dependent anticancer pathways. However, if PXR has already been activated, nelfinavir may antagonize this activation and result in tumor suppression or counteract PXR-induced chemoresistance. Here, PXR antagonism might synergize with other anticancer pathways, which are triggered by nelfinavir. It is the other way around in cancers, in which PXR acts as a tumor suppressor. Consequently, the here-described partial agonism and competitive antagonism of nelfinavir in the modulation of PXR activity have to be considered if nelfinavir is planned to be used as an anticancer drug.

In conclusion, we have elucidated the molecular mechanism of PXR modulation by nelfinavir and its major metabolite M8. Both compounds bind directly to the receptor and act as partial agonists but also competitively antagonize ligand-mediated PXR activation. Given the current efforts to repurpose nelfinavir as an anticancer drug and considering that PXR plays a role in cancer cell survival pathways and is thought to be involved in the development of chemoresistance, it is important to know how the drug influences PXR activity. The data presented here may thus help to achieve a better understanding of the manifold effects of nelfinavir on cancer cells.

Acknowledgments

We greatly appreciate the expert technical assistance of K. Abuazi Rincones (Stuttgart). M. Demmel and colleagues (Biobank, Munich) kindly prepared primary human hepatocytes. This work was supported by the Human Tissue and Cell Research (HTCR) Foundation, a nonprofit foundation regulated by German civil law, which facilitates research with human tissue through the provision of an ethical and legal framework for sample collection. B. Spiegelman, T. Tanaka, and H. Wang kindly provided plasmids.

Authorship Contributions

Participated in research design: Burk, Windshügel.
Conducted experiments: Burk, Kronenberger, Keminer, Windshügel.
Contributed new reagents or analytic tools: Lee, Schiergens.
Performed data analysis: Burk, Kronenberger, Keminer, Windshügel.
Wrote or contributed to the writing of the manuscript: Burk, Schwab, Windshügel.

References

Arnold KA, Eichelbaum M, and Burk O (2004) Alternative splicing affects the function and tissue-specific expression of the human constitutive androstane receptor. *Nucl Recept* **2**:1.
Basseville A, Preisser L, de Carné Trécesson S, Boisdron-Celle M, Gamelin E, Coqueret O, and Morel A (2011) Irinotecan induces steroid and xenobiotic receptor (SXR) signaling to detoxification pathway in colon cancer cells. *Mol Cancer* **10**:80.
Berman HM, Westbrook J, Feng Z, Gilliland G, Bhat TN, Weissig H, Shindyalov IN, and Bourne PE (2000) The protein data bank. *Nucleic Acids Res* **28**:235–242.
Bhattarai D, Singh S, Jang Y, Hyeon Han S, Lee K, and Choi Y (2016) An insight into drug repositioning for the development of novel anti-cancer drugs. *Curr Top Med Chem* **16**:2156–2168.
Bitter A, Rümmele P, Klein K, Kandel BA, Rieger JK, Nüssler AK, Zanger UM, Trauner M, Schwab M, and Burk O (2015) Pregnane X receptor activation and silencing promote steatosis of human hepatic cells by distinct lipogenic mechanisms. *Arch Toxicol* **89**:2089–2103.
Burgermeister E, Schnoebelen A, Flament A, Benz J, Stihle M, Gsell B, Rufer A, Ruf A, Kuhn B, Märki HP, et al. (2006) A novel partial agonist of peroxisome proliferator-activated receptor-gamma (PPARgamma) recruits PPARgamma-coactivator-1alpha, prevents triglyceride accumulation, and potentiates insulin signaling in vitro. *Mol Endocrinol* **20**:809–830.
Burk O, Arnold KA, Nussler AK, Schaeffeler E, Efimova E, Avery BA, Avery MA, Fromm MF, and Eichelbaum M (2005) Antimalarial artemisinin drugs induce cytochrome P450 and MDR1 expression by activation of xenosensors pregnane X receptor and constitutive androstane receptor. *Mol Pharmacol* **67**:1954–1965.
Burk O, Kuzikov M, Kronenberger T, Jeske J, Keminer O, Thasler WE, Schwab M, Wrenger C, and Windshügel B (2018) Identification of approved drugs as potent inhibitors of pregnane X receptor activation with differential receptor interaction profiles. *Arch Toxicol* **92**:1435–1451.
Burk O, Tegude H, Koch I, Hustert E, Wolbold R, Glaeser H, Klein K, Fromm MF, Nuessler AK, Neuhaus P, et al. (2002) Molecular mechanisms of polymorphic CYP3A7 expression in adult human liver and intestine. *J Biol Chem* **277**: 24280–24288.
De Gassart A, Bujisic B, Zaffalon L, Decosterd LA, Di Micco A, Frera G, Tallant R, and Martinon F (2016) An inhibitor of HIV-1 protease modulates constitutive eIF2α dephosphorylation to trigger a specific integrated stress response. *Proc Natl Acad Sci USA* **113**:E117–E126.
Dixit V, Hariparsad N, Li F, Desai P, Thummel KE, and Unadkat JD (2007) Cytochrome P450 enzymes and transporters induced by anti-human immunodeficiency virus protease inhibitors in human hepatocytes: implications for predicting clinical drug interactions. *Drug Metab Dispos* **35**:1853–1859.
Dong H, Lin W, Wu J, and Chen T (2010) Flavonoids activate pregnane x receptor-mediated CYP3A4 gene expression by inhibiting cyclin-dependent kinases in HepG2 liver carcinoma cells. *BMC Biochem* **11**:23.
Dussault I, Lin M, Hollister K, Wang EH, Synold TW, and Forman BM (2001) Peptide mimetic HIV protease inhibitors are ligands for the orphan receptor SXR. *J Biol Chem* **276**:33309–33312.
Feng F, Jiang Q, Cao S, Cao Y, Li R, Shen L, Zhu H, Wang T, Sun L, Liang E, et al. (2018) Pregnane X receptor mediates sorafenib resistance in advanced hepatocellular carcinoma. *Biochim Biophys Acta Gen Subj* **1862**:1017–1030.

Forman BM, Tontonoz P, Chen J, Brun RP, Spiegelman BM, and Evans RM (1995) 15-Deoxy-delta 12, 14-prostaglandin J2 is a ligand for the adipocyte determination factor PPAR gamma. *Cell* **83**:803–812.

Fujimura T, Sakuma H, Konishi S, Oe T, Hosogai N, Kimura C, Aramori I, and Mutoh S (2005) FK614, a novel peroxisome proliferator-activated receptor gamma modulator, induces differential transactivation through a unique ligand-specific interaction with transcriptional coactivators. *J Pharmacol Sci* **99**:342–352.

Geick A, Eichelbaum M, and Burk O (2001) Nuclear receptor response elements mediate induction of intestinal MDR1 by rifampin. *J Biol Chem* **276**:14581–14587.

Guan M, Fousek K, Jiang C, Guo S, Synold T, Xi B, Shih CC, and Chow WA (2011) Nelfinavir induces liposarcoma apoptosis through inhibition of regulated intramembrane proteolysis of SREBP-1 and ATF6. *Clin Cancer Res* **17**:1796–1806.

Gupta A, Mugundu GM, Desai PB, Thummel KE, and Unadkat JD (2008) Intestinal human colon adenocarcinoma cell line LS180 is an excellent model to study pregnane X receptor, but not constitutive androstane receptor, mediated CYP3A4 and multidrug resistance transporter 1 induction: studies with anti-human immunodeficiency virus protease inhibitors. *Drug Metab Dispos* **36**:1172–1180.

Gupta AK, Li B, Cerniglia GJ, Ahmed MS, Hahn SM, and Maity A (2007) The HIV protease inhibitor nelfinavir downregulates Akt phosphorylation by inhibiting proteasomal activity and inducing the unfolded protein response. *Neoplasia* **9**: 271–278.

Harmsen S, Meijerman I, Febus CL, Maas-Bakker RF, Beijnen JH, and Schellens JH (2010) PXR-mediated induction of P-glycoprotein by anticancer drugs in a human colon adenocarcinoma-derived cell line. *Cancer Chemother Pharmacol* **66**: 765–771.

Hoffart E, Ghebreghiorghis L, Nussler AK, Thasler WE, Weiss TS, Schwab M, and Burk O (2012) Effects of atorvastatin metabolites on induction of drug-metabolizing enzymes and membrane transporters through human pregnane X receptor. *Br J Pharmacol* **165**:1595–1608.

Huang L, Wring SA, Woolley JL, Brouwer KR, Serabjit-Singh C, and Polli JW (2001) Induction of P-glycoprotein and cytochrome P450 3A by HIV protease inhibitors. *Drug Metab Dispos* **29**:754–760.

Hustert E, Zibat A, Presecan-Siedel E, Eiselt R, Mueller R, Fuss C, Brehm I, Brinkmann U, Eichelbaum M, Wojnowski L, et al. (2001) Natural protein variants of pregnane X receptor with altered transactivation activity toward CYP3A4. *Drug Metab Dispos* **29**:1454–1459.

Jeske J, Windshügel B, Thasler WE, Schwab M, and Burk O (2017) Human pregnane X receptor is activated by dibenzazepine carbamate-based inhibitors of constitutive androstane receptor. *Arch Toxicol* **91**:2375–2390.

Jiang W, Mikochik PJ, Ra JH, Lei H, Flaherty KT, Winkler JD, and Spitz FR (2007) HIV protease inhibitor nelfinavir inhibits growth of human melanoma cells by induction of cell cycle arrest. *Cancer Res* **67**:1221–1227.

Jones K, Hoggard PG, Sales SD, Khoo S, Davey R, and Back DJ (2001) Differences in the intracellular accumulation of HIV protease inhibitors in vitro and the effect of active transport. *AIDS* **15**:675–681.

Kim JY, Park YJ, Lee BM, and Yoon S (2019) Co-treatment with HIV protease inhibitor nelfinavir greatly increases late-phase apoptosis of drug-resistant KBV20C cancer cells independently of P-glycoprotein inhibition. *Anticancer Res* **39**:3757–3765.

Koltai T (2015) Nelfinavir and other protease inhibitors in cancer: mechanisms involved in anticancer activity. *F1000 Res* **4**:9.

Laskowski RA, MacArthur MW, Moss DS, and Thornton JM (1993) PROCHECK-a program to check the stereochemical quality of protein structures. *J Appl Cryst* **26**:283–291.

Lee SM, Schelcher C, Demmel M, Hauner M, and Thasler WE (2013) Isolation of human hepatocytes by a two-step collagenase perfusion procedure. *J Vis Exp*:e50615.

Lin W, Wang YM, Chai SC, Lv L, Zheng J, Wu J, Zhang Q, Wang YD, Griffin PR, and Chen T (2017) SPA70 is a potent antagonist of human pregnane X receptor. *Nat Commun* **8**:741.

Lin W, Wu J, Dong H, Bouck D, Zeng FY, and Chen T (2008) Cyclin-dependent kinase 2 negatively regulates human pregnane X receptor-mediated CYP3A4 gene expression in HepG2 liver carcinoma cells. *J Biol Chem* **283**:30650–30657.

Liu L, Mugundu GM, Kirby BJ, Samineni D, Desai PB, and Unadkat JD (2012) Quantification of human hepatocyte cytochrome P450 enzymes and transporters induced by HIV protease inhibitors using newly validated LC-MS/MS cocktail assays and RT-PCR. *Biopharm Drug Dispos* **33**:207–217.

Lynch C, Zhao J, Huang R, Xiao J, Li L, Heyward S, Xia M, and Wang H (2015) Quantitative high-throughput identification of drugs as modulators of human constitutive androstane receptor. *Sci Rep* **5**:10405.

Mackowiak B and Wang H (2016) Mechanisms of xenobiotic receptor activation: direct vs. indirect. *Biochim Biophys Acta* **1859**:1130–1140.

Masuyama H, Suwaki N, Tateishi Y, Nakatsukasa H, Segawa T, and Hiramatsu Y (2005) The pregnane X receptor regulates gene expression in a ligand- and promoter-selective fashion. *Mol Endocrinol* **19**:1170–1180.

Mateus A, Treyer A, Wegler C, Karlgren M, Matsson P, and Artursson P (2017) Intracellular drug bioavailability: a new predictor of system dependent drug disposition. *Sci Rep* **7**:43047.

Oberfield JL, Collins JL, Holmes CP, Goreham DM, Cooper JP, Cobb JE, Lenhard JM, Hull-Ryde EA, Mohr CP, Blanchard SG, et al. (1999) A peroxisome proliferator-activated receptor gamma ligand inhibits adipocyte differentiation. *Proc Natl Acad Sci USA* **96**:6102–6106.

Pascussi JM, Gerbal-Chaloin S, Drocourt L, Maurel P, and Vilarem MJ (2003) The expression of CYP2B6, CYP2C9 and CYP3A4 genes: a tangle of networks of nuclear and steroid receptors. *Biochim Biophys Acta* **1619**:243–253.

Piedade R, Traub S, Bitter A, Nüssler AK, Gil JP, Schwab M, and Burk O (2015) Carboxymefloquine, the major metabolite of the antimalarial drug mefloquine, induces drug-metabolizing enzyme and transporter expression by activation of pregnane X receptor. *Antimicrob Agents Chemother* **59**:96–104.

Planque C, Rajabi F, Grillet F, Finetti P, Bertucci F, Gironella M, Lozano JJ, Beucher B, Giraud J, Garambois V, et al. (2016) Pregnane X-receptor promotes stem cell-mediated colon cancer relapse. *Oncotarget* **7**:56558–56573.

Pondugula SR, Pavek P, and Mani S (2016) Pregnane X receptor and cancer: context-specificity is key. *Nucl Receptor Res* **3**:101198.

Prakash C, Zuniga B, Song CS, Jiang S, Cropper J, Park S, and Chatterjee B (2015) Nuclear receptors in drug metabolism, drug response and drug interactions. *Nucl Receptor Res* **2**:101178.

Riedmaier S, Klein K, Hofmann U, Keskitalo JE, Neuvonen PJ, Schwab M, Niemi M, and Zanger UM (2010) UDP-glucuronosyltransferase (UGT) polymorphisms affect atorvastatin lactonization in vitro and in vivo. *Clin Pharmacol Ther* **87**:65–73.

Shim JS and Liu JO (2014) Recent advances in drug repositioning for the discovery of new anticancer drugs. *Int J Biol Sci* **10**:654–663.

Shim JS, Rao R, Beebe K, Neckers L, Han I, Nahta R, and Liu JO (2012) Selective inhibition of HER2-positive breast cancer cells by the HIV protease inhibitor nelfinavir. *J Natl Cancer Inst* **104**:1576–1590.

Singh VP, Bren GD, Algeciras-Schimnich A, Schnepple D, Navina S, Rizza SA, Dawra RK, Saluja AK, Chari ST, Vege SS, et al. (2009) Nelfinavir/ritonavir reduces acinar injury but not inflammation during mouse caerulein pancreatitis. *Am J Physiol Gastrointest Liver Physiol* **296**:G1040–G1046.

Sippl MJ (1993) Recognition of errors in three-dimensional structures of proteins. *Proteins* **17**:355–362.

Svärd J, Spiers JP, Mulcahy F, and Hennessy M (2010) Nuclear receptor-mediated induction of CYP450 by antiretrovirals: functional consequences of NR1I2 (PXR) polymorphisms and differential prevalence in whites and sub-Saharan Africans. *J Acquir Immune Defic Syndr* **55**:536–549.

Tachibana K, Kobayashi Y, Tanaka T, Tagami M, Sugiyama A, Katayama T, Ueda C, Yamasaki D, Ishimoto K, Sumitomo M, et al. (2005) Gene expression profiling of potential peroxisome proliferator-activated receptor (PPAR) target genes in human hepatoblastoma cell lines inducibly expressing different PPAR isoforms. *Nucl Recept* **3**:3.

Thasler WE, Weiss TS, Schillhorn K, Stoll PT, Irrgang B, and Jauch KW (2003) Charitable state-controlled foundation Human Tissue and Cell Research: ethic and legal aspects in the supply of surgically removed human tissue for research in the academic and commercial sector in Germany. *Cell Tissue Bank* **4**:49–56.

Wang H, Faucette S, Sueyoshi T, Moore R, Ferguson S, Negishi M, and LeCluyse EL (2003) A novel distal enhancer module regulated by pregnane X receptor/constitutive androstane receptor is essential for the maximal induction of CYP2B6 gene expression. *J Biol Chem* **278**:14146–14152.

Wang H, Li H, Moore LB, Johnson MD, Maglich JM, Goodwin B, Ittoop OR, Wisely B, Creech K, Parks DJ, et al. (2008) The phytoestrogen coumestrol is a naturally occurring antagonist of the human pregnane X receptor. *Mol Endocrinol* **22**:838–857.

Wignot TM, Stewart RP, Schray KJ, Das S, and Sipos T (2004) In vitro studies of the effects of HAART drugs and excipients on activity of digestive enzymes. *Pharm Res* **21**:420–427.

Xie L, Evangelidis T, Xie L, and Bourne PE (2011) Drug discovery using chemical systems biology: weak inhibition of multiple kinases may contribute to the anticancer effect of nelfinavir. *PLOS Comput Biol* **7**:e1002037.

Xing Y, Yan J, and Niu Y (2020) PXR: a center of transcriptional regulation in cancer. *Acta Pharm Sin B* **10**:197–206.

Yasuda M, Kishimoto S, Amano M, and Fukushima S (2019) The Involvement of pregnane X receptor-regulated pathways in the antitumor activity of cisplatin. *Anticancer Res* **39**:3601–3608.

Zhang KE, Wu E, Patick AK, Kerr B, Zorbas M, Lankford A, Kobayashi T, Maeda Y, Shetty B, and Webber S (2001) Circulating metabolites of the human immunodeficiency virus protease inhibitor nelfinavir in humans: structural identification, levels in plasma, and antiviral activities. *Antimicrob Agents Chemother* **45**:1086–1093.

Address correspondence to: Oliver Burk, Dr. Margarete Fischer-Bosch-Institute of Clinical Pharmacology, Auerbachstrasse 112, 70376 Stuttgart, Germany. E-mail oliver.burk@ikp-stuttgart.de; or Björn Windshügel, Fraunhofer Institute for Molecular Biology and Applied Ecology IME, ScreeningPort, Schnackenburgallee 114, 22525 Hamburg, Germany. E-mail bjoern.windshuegel@ime.fraunhofer.de

Supplemental Data

Manuscript number: MOLPHARM-AR-2020-000116R1

Nelfinavir and its active metabolite M8 are partial agonists and competitive antagonists of the human pregnane X receptor

Oliver Burk, Thales Kronenberger, Oliver Keminer, Serene M. L. Lee, Tobias S. Schiergens, Matthias Schwab, Björn Windshügel

Supplemental Materials and Methods

Cell viability

HepG2 or H-P cells were seeded into white flat-bottom CELLSTAR® 96-well plates with µClear® bottom (Greiner Bio-One, Frickenhausen, Germany), with 40,000 cells per well in a volume of 100 µl and incubated for 24 hours. Then, cells were treated for further 24 hours with varying doses of nelfinavir or metabolite M8, ranging from 1 to 50 µM, or vehicle only (0.5% DMSO). Each treatment was performed in technical triplicates. Afterwards, cell viability was determined based on ATP content, using the CellTiter-Glo® luminescent cell viability assay (Promega), as specified by the manufacturer. Luminescence was measured with the 2300 EnSpire multimode plate reader (Perkin Elmer, Rodgau, Germany).

Supplemental Table S1 Hepatocyte donor data

ID	ethnicity	sex	age cohort	diagnosis	long-term medication	used in
GH41	European	female	30-39	liver metastasis CRC	n.s.	Fig. 7A
GH42	European	female	50-59	focal nodular hyperplasia	none	Fig. 7A
GH43	European	female	30-39	focal nodular hyperplasia	n.s.	Fig. 7A
GH44	European	male	50-59	liver metastasis CRC	vitamin D	Fig. 7A
GH45	European	female	60-69	liver metastasis CRC	pantoprazole	Fig. 7A
GH46	n.s.	Male	30-39	liver metastasis CRC	pantoprazole	Fig. 7A
GH61	n.s.	female	70-79	liver metastasis breast carcinoma	ramipril, L-thyroxine	Fig. 7B
GH62	European	Male	70-79	liver metastasis CRC	acetylsalicylic acid, bisoprolol, simvastatin, ticagrelor	Fig. 7B
GH63	European	Female	30-39	liver metastasis CRC	tinzaparin	Fig. 7B
GH64	European	Male	60-69	intrahepatic CCC	salbutamol, unspecified hypertensive drug(s), unspecified ACE inhibitor(s)	Fig. 7B

n.s., not specified; CRC, colorectal carcinoma; CCC, cholangiocellular carcinoma

Supplemental Table S2. Overview of binding site characteristics and docking scores.

PDB ID	Pocket	Size	PLB	Docking Scores	
				NFV	M8
1M13	LBP	245	4.6	101.4	104.3
C284 A	AF-2	n.d.	n.d.	77.07	76.2
	Alt-1	60	1.4	82.9	80.3
	Alt-2	56	0.8	68.4	71
1M13	LBP	244	4.6	104.4	106.1
C284 B	AF-2	n.d.	n.d.	75.3	74.8
	Alt-1	60	1.48	78.1	80.7
	Alt 2	64	0.91	66.7	67.8
1NRL	LBP	190	4.4	107.4	110.4
Chain A	AF-2	n.d.	n.d.	76.8	78
	Alt-1	32	1.37	64.7	67.4
	Alt-2	45	1.16	71	66.8
1NRL	LBP	190	3.8	97	100
Chain B	AF-2	n.d.	n.d.	81.1	78.2
	Alt-1	67	1.9	63.7	68.2
	Alt-2	41	1.2	76.3	78.3
2O9I	LBP	186	4	104	103.2
Chain A	AF-2	n.d.	n.d.	75.3	78.5
	Alt-1	52	1.8	73.4	72.1
	Alt-2	46	1	73.9	75.1
2O9I	LBP	186	4	98.4	101
Chain B	AF-2	n.d.	n.d.	84.2	85.4
	Alt-1	52	1.8	65.2	63.7
	Alt-2	46	1	70.3	79.3

For the PXR LBD structures used in this study, the calculated size (number of alpha spheres) of the LBP, AF-2 groove, and the alternative pockets (Alt-1, Alt-2) are listed, along with the calculated propensity for ligand binding (PLB) at these sites. For each pocket, the top-ranked docking scores of nelfinavir (NFV) and M8 are provided. n.d., not determined.

Supplemental Table S3. Number of docking poses per cluster and their ranking according to the docking score within the set of 100 docking conformations

Cluster	Nelfinavir		M8	
	Cluster Size	Docking Poses	Cluster Size	Docking Poses
1	8	1,2,4,5,6,8,16,51	4	1,2,5,11
2	1	3	4	3,4,24,27
3	4	7,9,13,14	3	6,12,42
4	1	10	4	7,9,21,32
			3	8,16,73
			1	10

Supplemental Table S4 Rifampin EC_{50} with increasing doses of nelfinavir and M8

NFV	Rifampin		M8	Rifampin	
[µM]	EC_{50} [µM]	95% CI [µM]	[µM]	EC_{50} [µM]	95% CI [µM]
0	2.0	1.2 - 3.3	0	1.6	0.97 - 2.7
3	5.4	3.4 – 8.8	3	2.1	1.1 - 4.1
10	19.7	6.9 - 158	10	5.9	5.4 - ???

???, not computable by GraphPad Prism

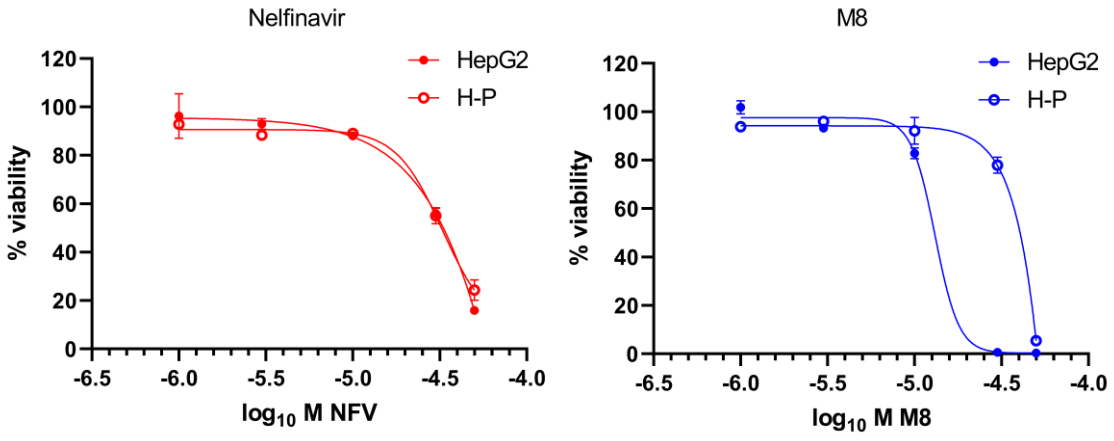

Supplemental Fig. S1. Cell toxicity of nelfinavir and M8. HepG2 and H-P cells were treated with increasing concentrations of nelfinavir or M8 metabolite for 24 h. Means ± SD (*N*=2) are shown.

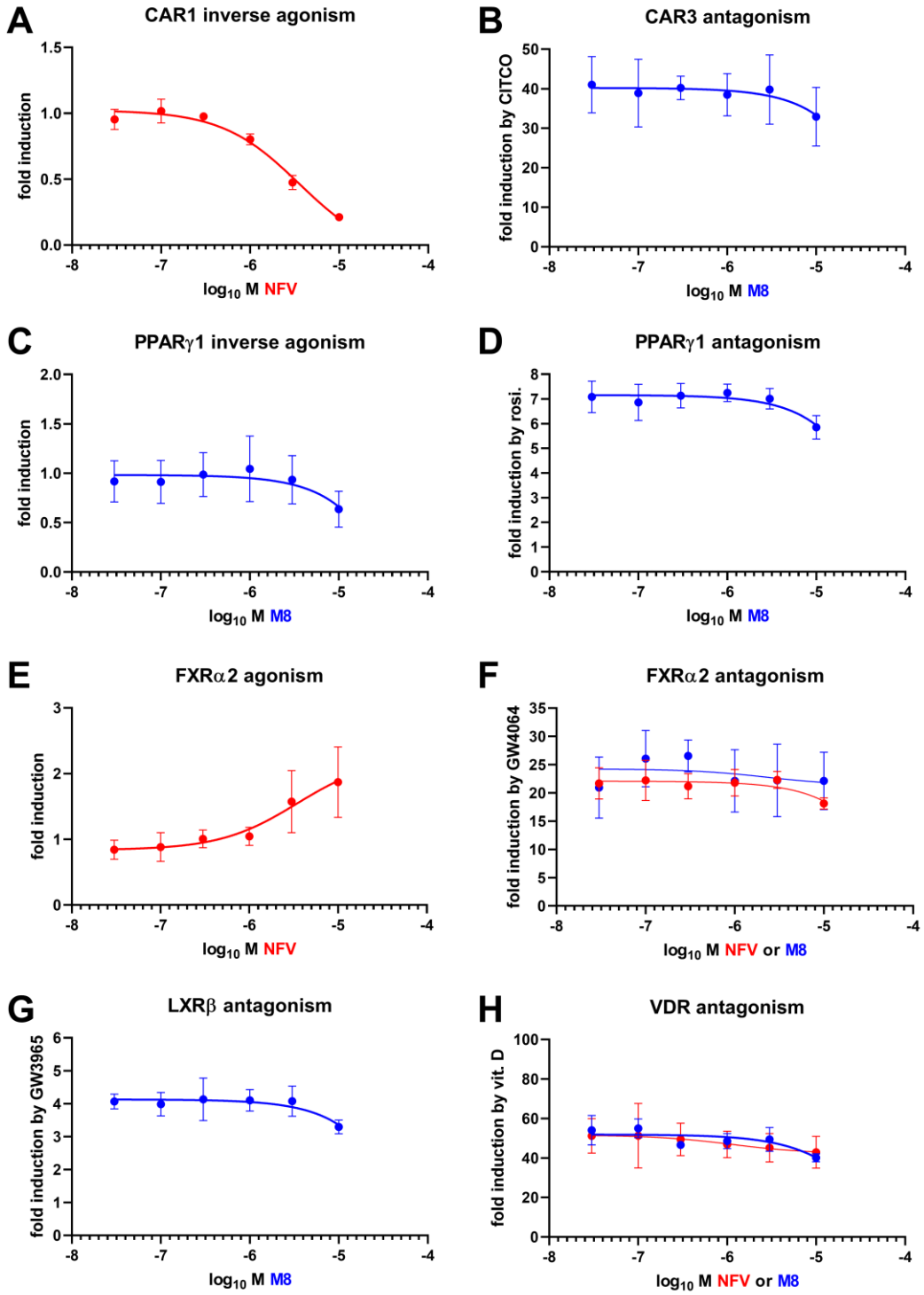

Supplemental Fig. S2. Concentration response analyses of the effects of nelfinavir and/or M8 on nuclear receptors beside PXR. HepG2 cells were co-transfected with expression plasmids encoding human CAR1 (A), CAR3 (B), PPARγ1 (C, D), FXRα2 (E, F), LXRβ (G) or VDR (H) and the corresponding reporter gene plasmids (see Materials and Methods). Transfected cells were treated with increasing concentrations of nelfinavir (NFV) or M8, alone (A, C, E) or in combination with respective receptor agonists (B, D, F-H), as indicated. Mean fold induction ± SD (*n*=3) by the respective treatment is shown, with respect to the normalized reporter activity of cells treated with vehicle DMSO only, which was designated as 1. Non-linear fit of dose response was executed as described in Materials and Methods. rosi., rosiglitazone; vit. D, 1α,25-dihydroxyvitamin D3.

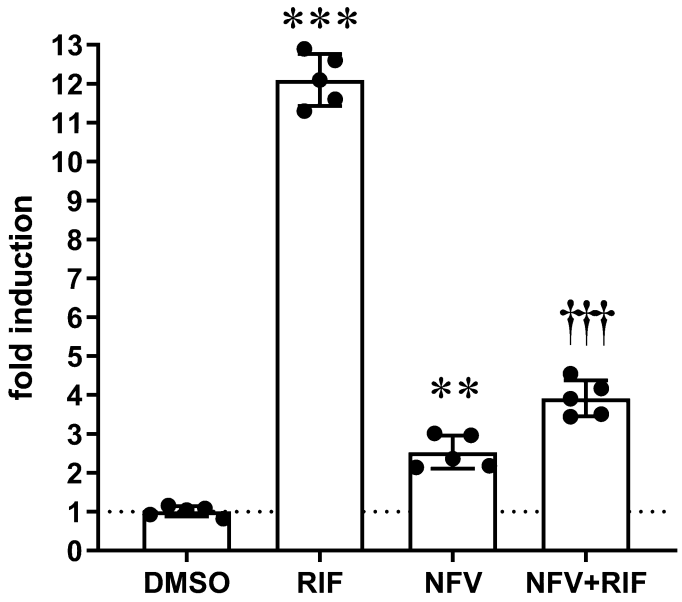

Supplemental Fig. S3. Effect of nelfinavir on the GAL4-PXR-LBD fusion protein. HepG2 cells were transfected with expression plasmid encoding GAL4-DBD/PXR-LBD(108-434) fusion protein. Transfected cells were treated with 0.1% DMSO or 10 µM nelfinavir (NFV) in the absence or presence of 10 µM rifampin (RIF) for 24h. Data are presented as scatter plots with means (columns) ± S.D. (*n*=5) of normalized luciferase activity of co-transfected pGL3-G5, relative to the activity of cells treated with vehicle DMSO only. Differences to respective treatments with DMSO (asterisks, exclusively for single compound treatments) or rifampin alone (daggers, exclusively for rifampin co-treatment) were analyzed by repeated measures one-way ANOVA with Dunnett's multiple comparisons test or paired t-test, respectively.

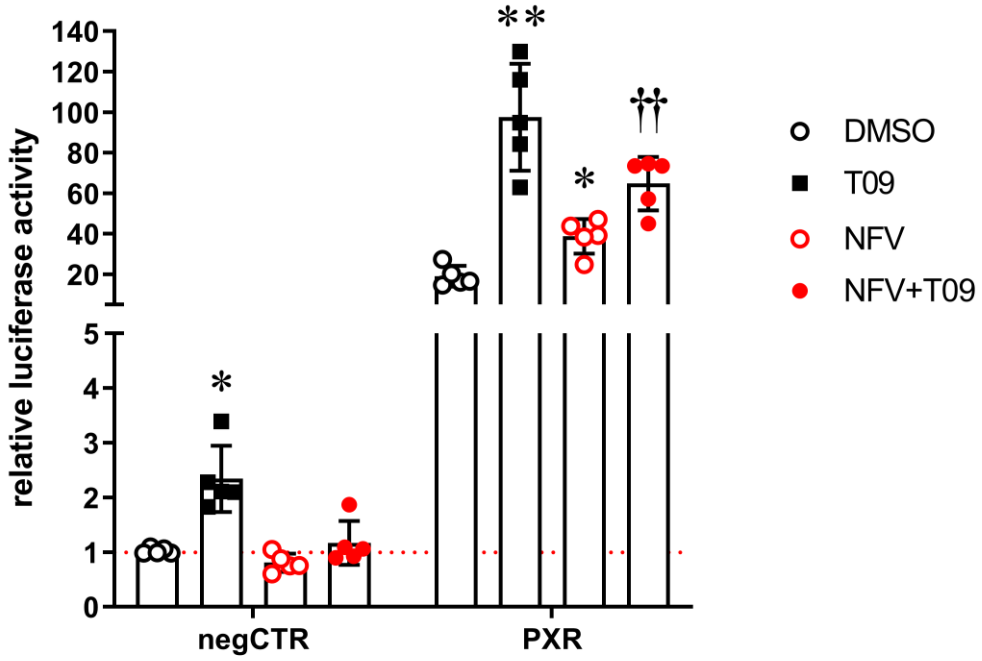

Supplemental Fig. S4. Effect of nelfinavir on PXR activation by the high affinity agonist T0901317. HepG2 cells were transfected with empty vector pcDNA3 (negCTR) or expression plasmid encoding human PXR and treated with 0.1% DMSO or 10 µM nelfinavir (NFV), with or without 1 µM T0901317 (T09) for 24 h. Data are presented in scatter plots with means (columns) ± SD (n=5) of normalized luciferase activity of co-transfected CYP3A4 reporter, relative to the activity of cells transfected with pcDNA3 and treated with DMSO only. Differences to respective treatments with DMSO (asterisks, exclusively for single compound treatments) or T0901317 alone (daggers, exclusively for T0901317 co-treatments) were analyzed by repeated measures two-way ANOVA with Dunnett's multiple comparisons test. *, P<0.05; **, †† P<0.01.